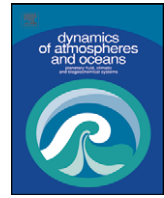




ELSEVIER

Contents lists available at ScienceDirect

Dynamics of Atmospheres and Oceans

journal homepage: www.elsevier.com/locate/dynatmoce

The Gulf Stream pathway and the impacts of the eddy-driven abyssal circulation and the Deep Western Boundary Current

Harley E. Hurlburt*, Patrick J. Hogan

Naval Research Laboratory, Stennis Space Center, MS 39529, USA

ARTICLE INFO

Article history:

Available online 6 July 2008

Keywords:

Ocean circulation
 Western boundary currents
 Oceanic fronts
 Abyssal circulation
 Bottom topography effects
 Western North Atlantic Ocean
 Gulf Stream region

ABSTRACT

A hydrodynamic model of the subtropical Atlantic basin and the Intra-Americas Sea (9–47°N) is used to investigate the dynamics of Gulf Stream separation from the western boundary at Cape Hatteras and its mean pathway to the Grand Banks. The model has five isopycnal Lagrangian layers in the vertical and allows realistic boundary geometry, bathymetry, wind forcing, and a meridional overturning circulation (MOC), the latter specified via ports in the northern and southern boundaries. The northward upper ocean branch of the MOC (14 Sv) was always included but the southward Deep Western Boundary Current (DWBC) was excluded in some simulations, allowing investigation of the impacts of the DWBC and the eddy-driven mean abyssal circulation on Gulf Stream separation from the western boundary. The result is resolution dependent with the DWBC playing a crucial role in Gulf Stream separation at 1/16° resolution but with the eddy-driven abyssal circulation alone sufficient to obtain accurate separation at 1/32° resolution and a realistic pathway from Cape Hatteras to the Grand Banks with minimal DWBC impact except southeast of the Grand Banks. The separation from the western boundary is particularly sensitive to the strength of the eddy-driven abyssal circulation. Farther to the east, between 68°W and the Grand Banks, all of the 1/16° and 1/32° simulations with realistic topography (with or without a DWBC) gave similar generally realistic mean pathways with clear impacts of the topographically constrained eddy-driven abyssal circulation versus very unrealistic Gulf Stream pathways between Cape Hatteras and the Grand Banks from otherwise identical simulations run with a flat bottom, in reduced-gravity mode, or with 1/8° resolution and

* Corresponding author. Tel.: +1 228 688 4626; fax: +1 228 688 4759.

E-mail addresses: hurlburt@nrlssc.navy.mil (H.E. Hurlburt), hogan@nrlssc.navy.mil (P.J. Hogan).

realistic topography. The model is realistic enough to allow detailed model-data comparisons and a detailed investigation of Gulf Stream dynamics. The corresponding linear solution with a Sverdrup interior and Munk viscous western boundary layers, including one from the northward branch of the MOC, yielded two unrealistic Gulf Stream pathways, a broad eastward pathway centered at the latitude of Cape Hatteras and a second wind plus MOC-driven pathway hugging the western boundary to the north. Thus, a high resolution model capable of simulating an inertial jet is required to obtain a single nonlinear Gulf Stream pathway as it separates from the coast. None of the simulations were sufficiently inertial to overcome the linear solution need for a boundary current north of Cape Hatteras without assistance from pathway advection by the abyssal circulation, even though the core speeds of the simulated currents were consistent with observations near separation. In the $1/16^\circ$ simulation with no DWBC and a $1/32^\circ$ simulation with high bottom friction and no DWBC the model Gulf Stream overshoot the observed separation latitude. With abyssal current assistance the simulated (and the observed) mean Gulf Stream pathway between separation from the western boundary and $\sim 70^\circ\text{W}$ agreed closely with a constant absolute vorticity (CAV) trajectory influenced by the angle of the coastline prior to separation. The key abyssal current crosses under the Gulf Stream at $68.5\text{--}69^\circ\text{W}$ and advects the Gulf Stream pathway southward to the terminus of an escarpment in the continental slope. There the abyssal current crosses to deeper depths to conserve potential vorticity while passing under the downward-sloping thermocline of the stream and then immediately retroflects eastward onto the abyssal plain, preventing further southward pathway advection. Thus specific topographic features and feedback from the impact of the Gulf Stream on the abyssal current pathway determined the latitude of the stream at $68.5\text{--}69^\circ\text{W}$, a latitude verified by observations. The associated abyssal current was also verified by observations.

Published by Elsevier B.V.

1. Introduction

There have been numerous theories and modeling studies of Gulf Stream separation from the western boundary at Cape Hatteras and its pathway to the Grand Banks of Newfoundland, as discussed in reviews by Dengg et al. (1996) and by Chassignet and Marshall (2008). These studies have used models ranging from highly idealized to complex ocean general circulation models (OGCMs) designed for realistic simulation of a wide range of ocean processes. Significant progress has been made, especially in realistic simulation of Gulf Stream separation from the western boundary and its subsequent pathway to the east when using realistic boundary geometry, bathymetry, wind forcing, meridional overturning and equatorial resolution of $1/10^\circ$ (8.5 km at 40°N) or finer (Paiva et al., 1999; Hurlburt and Hogan, 2000; Smith et al., 2000; Bryan et al., 2007; Chassignet and Marshall, 2008). However, as noted by Chassignet and Marshall (2008), “identifying the dynamics responsible for Gulf Stream separation continues to be a challenge”.

Most previous modeling studies of the Gulf Stream have used either a very idealized model or a complex OGCM. Here we take a significantly different approach based on a model that is intermediate between highly idealized and a complex OGCM, the model used by Hurlburt and Hogan (2000). The model retains all of the key features noted above that were included in models that yielded realistic simulations of the Gulf Stream, but it is purely hydrodynamic and has only five isopycnal Lagrangian layers in the vertical. Thus, it is feasible to perform a substantial suite of simulations with mid-latitude horizontal resolution as fine as $1/64^\circ$ (1.8 km for each variable). This approach also facilitates experimental design and interpretation of the results. The model is realistic enough to allow detailed model-data

comparisons and thus provide a strong observational basis to assess findings from the model results. While Hurlburt and Hogan (2000) focused on model-data comparisons as a function of horizontal resolution, here the focus is Gulf Stream dynamics. Additional model-data comparisons are performed to assist in detailed evaluation and interpretation of the model dynamics and to assess the applicability of the model results in explaining Gulf Stream separation from the western boundary and its pathway to the east. The findings of Hurlburt and Hogan (2000) provide a useful foundation for this purpose, particularly since the two studies share a small, but key subset of the simulations they utilize.

Hurlburt and Hogan (2000) used numerous model-data comparisons to investigate whether it is possible to make nonlinear numerical models realistically simulate the Gulf Stream pathway and other aspects of the Gulf Stream system by simply increasing the horizontal grid resolution, while decreasing the eddy viscosity and better resolving the bottom topography in the process. Using the resolution sequence $1/8^\circ$, $1/16^\circ$, $1/32^\circ$ and $1/64^\circ$, they found that $1/16^\circ$ was the minimum for realistic results, but significant improvement was obtained by increasing the resolution to $1/32^\circ$ and more modest improvement by a further increase to $1/64^\circ$. The improvements at $1/16^\circ$ resolution and higher included (1) realistic separation of the Gulf Stream from the coast at Cape Hatteras and a realistic Gulf Stream pathway between Cape Hatteras and the Grand Banks based on comparisons with Gulf Stream pathways from the satellite infrared (IR) sea surface temperature (SST) front and from Geosat and TOPEX/Poseidon altimetry (but $1/32^\circ$ resolution was required for robust results), (2) realistic eastern and western nonlinear recirculation gyres (which contribute to the large-scale C-shape of the subtropical gyre) based on comparisons with mean surface dynamic height from the Generalized Digital Environmental Model (GDEM) oceanic climatology (described by Teague et al., 1990) and from the pattern and amplitude of SSH variability surrounding the eastern gyre as seen in TOPEX/Poseidon altimetry, (3) realistic upper ocean and Deep Western Boundary Current transports based on several types of measurements, (4) patterns and amplitude of SSH variability that were generally realistic compared to TOPEX/Poseidon altimetry, but that varied from simulation to simulation for specific features and were most realistic overall in the $1/64^\circ$ simulation, (5) a basin-wide explosion in the number and strength of mesoscale eddies (with warm core rings (WCRs) north of the Gulf Stream, the regional eddy features best observed by satellite IR), (6) realistic statistics for WCRs north of the Gulf Stream based on comparison to IR analyses (low at $1/16^\circ$ resolution and most realistic at $1/64^\circ$ resolution for mean population and rings generated/year; realistic ring diameters at all resolutions), and (7) realistic patterns and amplitude of abyssal EKE in comparison to historical measurements from current meters.

Design of the model configurations and model experiments are discussed in Section 2, including a theory used as one way of investigating Gulf Stream dynamics. Section 3 is focused on Gulf Stream dynamics and the use of observations to assess the simulated dynamics. In Section 4 flat bottom and reduced-gravity simulations further highlight the profound impact of topography on Gulf Stream simulations and their dynamics. Summary and conclusions follow in Section 5.

2. Ocean models and simulations

The numerical simulations were performed using the Naval Research Laboratory (NRL) layered ocean model (NLOM). General details of NLOM design and progressive development are discussed in Hurlburt and Thompson (1980), Wallcraft (1991), Wallcraft and Moore (1997), Moore and Wallcraft (1998), and Wallcraft et al. (2003). The last of these discusses the development of NLOM as a thermodynamic model with a Kraus and Turner (1967) type bulk mixed layer and SST. Different versions and configurations of NLOM have been used in a variety of Gulf Stream studies, as discussed in Hurlburt and Hogan (2000). Of those, several focused on aspects of Gulf Stream dynamics (Hurlburt and Thompson, 1984; Thompson and Schmitz, 1989; Schmitz and Thompson, 1993; Spall, 1996a,b; Townsend et al., 2000). Since Hurlburt and Hogan (2000) the thermodynamic version of NLOM has been used in two operational, eddy-resolving global ocean prediction systems (Smedstad et al., 2003; Shriver et al., 2007) and both of the preceding publications include discussion of the Gulf Stream.

NLOM is a primitive equation (PE) layered formulation where the model equations have been vertically integrated through each layer and, in the hydrodynamic configuration used here, all of the layers are isopycnal. The model equations for this configuration are given and discussed in Hurlburt and Hogan (2000). The model allows diapycnal mixing (mixing of mass and momentum between layers,

but not heat in a hydrodynamic configuration) and it allows ventilation of the layers (isopycnal outcropping). This capability is essential to permit cross-layer closed mean vertical circulations within the model domain and to allow thin layers near the surface. In essence, when any layer above the bottom layer becomes thinner than a chosen minimum thickness, water from the layer below is entrained into it at a velocity needed to maintain that minimum layer thickness. Mass and volume are conserved within each layer by requiring no net transfer of mass across a layer interface. The model equations are integrated on a C-grid using a semi-implicit numerical scheme to permit a longer time step, as discussed in Hurlburt and Thompson (1980).

The model can include vertically compressed but otherwise realistic bottom topography confined to the lowest layer. The compressed topography is calculated using:

$$d_c = d_r + a_t(d - d_r) \quad (1)$$

where d_c is the depth of the compressed topography in the model, d_r is a reference depth, a_t is the fractional amplitude of the topography above d_r , and d is the depth without compression. Here $d_r = 6500$ m, $a_t = 0$ for a flat bottom, $a_t = 1$ for uncompressed topography, and $a_t = .82$ in the simulations with variable-depth topography. Sill depths of shallow straits are maintained by constraining flow to small values below the sill depth in all of the simulations used here, e.g. see Metzger and Hurlburt (1996) for discussion.

This approach to reduction in topographic amplitude has little effect on three of the main reasons for including bottom topography (abyssal currents following geostrophic contours of the topography, regulation of baroclinic instability, and upper ocean – topographic coupling via mixed baroclinic–barotropic instabilities) in regions where the two-layer theory, described below, is valid. This coupling allows eddy-driven abyssal currents (and thus, the bottom topography) to steer the pathways of upper ocean currents that do not directly impinge on the topography, including their mean pathways (Hurlburt et al., 1996, 2008; Hurlburt and Metzger, 1998; Hogan and Hurlburt, 2000, 2005; Tilburg et al., 2001). Abyssal currents driven by any means can steer the pathways of upper ocean currents (Hurlburt and Thompson, 1980, 1982; Thompson and Schmitz, 1989).

Hurlburt and Thompson (1980) used the layered continuity equation and geostrophy in a two-layer model to show how lower layer currents could advect the pathways of upper layer currents in the model. In a two-layer model with no diapycnal mixing, the continuity equation for layer 1 is

$$h_{1t} + \mathbf{v}_1 \cdot \nabla h_1 + h_1 \nabla \cdot \mathbf{v}_1 = 0 \quad (2)$$

where h_1 is upper layer thickness, t is the time derivative and \mathbf{v}_i is the velocity in layer i . The geostrophic component of the advective term in (2) can be related to the geostrophic velocity (\mathbf{v}_{1g}) in layer 2 by

$$\mathbf{v}_{1g} \cdot \nabla h_1 = \mathbf{v}_{2g} \cdot \nabla h_1 \quad (3)$$

because from geostrophy,

$$\mathbf{k} \times f(\mathbf{v}_{1g} - \mathbf{v}_{2g}) = -g' \nabla h_1 \quad (4)$$

and thus $\mathbf{v}_{1g} - \mathbf{v}_{2g}$ is parallel to contours of h_1 . In (4) \mathbf{k} is a unit vector, $f = 2\omega \sin \theta$ is the Coriolis parameter, ω is the Earth's rotation rate ($7.292 \times 10^{-5} \text{ s}^{-1}$), θ is latitude, $g' = g(\rho_2 - \rho_1)/\rho_2$ is the reduced gravity due to buoyancy, $g = 9.8 \text{ m s}^{-2}$ is the gravitational acceleration of the Earth, and ρ_i is the water density in layer i . Since geostrophy is typically a very good approximation outside the equatorial wave guide and normally near-surface flows are much stronger than abyssal ocean flows, then usually $|\mathbf{v}_1| \gg |\mathbf{v}_2|$, making ∇h_1 a good measure of \mathbf{v}_1 under these conditions. Thus, the result that geostrophically balanced abyssal currents advect upper layer thickness gradients and therefore can advect the pathway of upper layer currents in a two-layer model, especially where relatively strong abyssal currents intersect upper layer currents at large angles. Further pathway advection is halted when a balance occurs between the divergence and advective terms in (2). In some cases the abyssal current steering results in abyssal and upper ocean currents that become more nearly parallel, because the current pathway advection is reduced when that occurs. This process results in a tendency towards barotropy.

See Hurlburt et al. (2008) for a more comprehensive discussion of the two-layer theory, including its limitations and its application to models with high vertical resolution and topography extending through any number of layers in the vertical. Near geostrophic balance, low vertical mode structure of

Table 1
Description and design characteristics of the Atlantic simulations

Resolution ^a			A (m ² s ⁻¹) ^b	C _b ^c	Bottom topog. ^d	DWBC ^e	Years spanned ^f	Figures where used ^g
Latitude θ	Longitude \emptyset	# layers						
1/16°	45/512°	1.5	30	NA	RG	No	152–180	Fig. 1 (linear)
1/8°	45/256°	5	100	.002	BT	Yes	106–125	Fig. 4b
1/16°	45/512°	5	20	.002	BT	Yes	55–66	Figs. 2a, 3a, 6a
1/16°	45/512°	5	20	.002	BT	No	91–109	Figs. 2b, 3b, 6b
1/32°	45/1024°	5	10	.002	BT	Yes	84–98	Figs. 2c, 3c, 4a, 5, 6c
1/32°	45/1024°	5	10	.002	BT	No	96–103	Figs. 2d, 3d, 6d
1/32°	45/1024°	5	10	.02	BT	Yes	100–107	Figs. 2e, 3e, 6e
1/32°	45/1024°	5	10	.02	BT	No	108–114	Figs. 2f, 3f, 6f
1/32°	45/1024°	5	10	.002	BT, no NESC	Yes	96–104	Fig. 8a and b
1/32°	45/1024°	5	10	.002	FB	Yes	128–145	Fig. 9a and b
1/32°	45/1024°	5	10	.02	FB	Yes	108–117	Fig. 9c and d
1/32°	45/1024°	4.5	10	NA	RG	No	41–58	Fig. 10a, b, and c

^a Resolution for each prognostic variable. The convention for reduced-gravity simulations is to call the inert, infinitely deep bottom layer half a layer.

^b A, Laplacian coefficient of isopycnal eddy viscosity.

^c C_b, coefficient of quadratic bottom friction, not applicable (NA) for the reduced-gravity (RG) simulations.

^d BT for realistic bottom topography confined to the lowest layer, Eq. (1), FB for flat bottom, and RG for reduced gravity. With a few exceptions, like the Gulf of Mexico, the 200 m isobath near the shelf break is used as the model boundary. Flow through shallow straits is constrained to small values below the sill depth in all of the simulations.

^e The upper ocean northward flow of the meridional overturning circulation (MOC) is included in all of the simulations.

^f The simulations were initialized from a simulation of compatible design already spun up to statistical equilibrium at the same or coarser resolution to minimize additional large-scale spin-up. The new simulations were monitored for convergence to a new statistical equilibrium and then run at least 4 more years. The years earlier than the model “years spanned” by each simulation were covered by parent simulation(s) with year 1 starting from rest. Means shown in the figures are generally formed over the last 4 years or more of a simulation. The domain-averaged thickness of each of the top four layers is 250 m. Using a thick abyssal layer greatly reduced the spin-up time required. The model is purely hydrodynamic with constant density in each layer and with density stratification [$\rho_{k+1} - \rho_k$ (in kg m⁻³)] of 1.01, .40, .31, .41 for layer interfaces 1–4, respectively, and 1.76 at 250 m depth for the 1.5 layer RG simulation, where k is the layer number counting downward. The stratification was derived using domain averages from the Levitus (1982) ocean climatology and the mean interface depths from an earlier spun-up simulation with a similar domain and layer structure.

^g The model experiments are identified by their latitudinal resolution and the first figure panel where they are used. Exp. 1/16°-1 has linear dynamics and all the rest are nonlinear. Fig. 1 (Exp. 1/16°-1) is a subregion of Fig. 7b in Townsend et al. (2000) that is designed to match the 9–47°N Atlantic model domain used for the nonlinear simulations. It is actually the linear superposition of separate linear simulations forced by winds and the northward branch of the MOC. Three of the nonlinear simulations were used in Hurlburt and Hogan (2000). Exps. 1/8°-4b, 1/16°-2a, and 1/32°-2c are 8H, 16H, and 32H, respectively, in Hurlburt and Hogan (2000), where they were subjected to numerous model-data comparisons. The remainder of the simulations have not been used in previous publications.

the flow, and topography that does not intrude significantly into the stratified water column are key requirements for application of the two-layer theory. This theory, as applied to steering of the mean Gulf Stream pathway by the eddy-driven mean abyssal circulation and the DWBC, is very useful in explaining the Gulf Stream pathway and its separation from the coast at Cape Hatteras.

All of the model simulations use kinematic and no slip boundary conditions. For currents along a model boundary, no slip conditions are important for boundary current separation because they generate a viscous sublayer not present with free slip conditions. The viscous sublayer facilitates inertial jet separation from a boundary by allowing relative vorticity advection of opposite sign on each side of the current maximum (Dengg, 1993; Özgökmen et al., 1997). However accurate numerical representation of the viscous sublayer is also required to avoid large errors in boundary current separation (Verron and Blayo, 1996; Wallcraft et al., 2005). Using Laplacian eddy viscosity, the viscous sublayer layer on the inshore side of the current maximum is resolved by four (nine) grid points in the nonlinear 1/16° (1/32°) simulations studied here.

The model experiments used in this investigation are summarized in Table 1. They are identified by their latitudinal resolution and the figure panel where they are first used. The experiments are

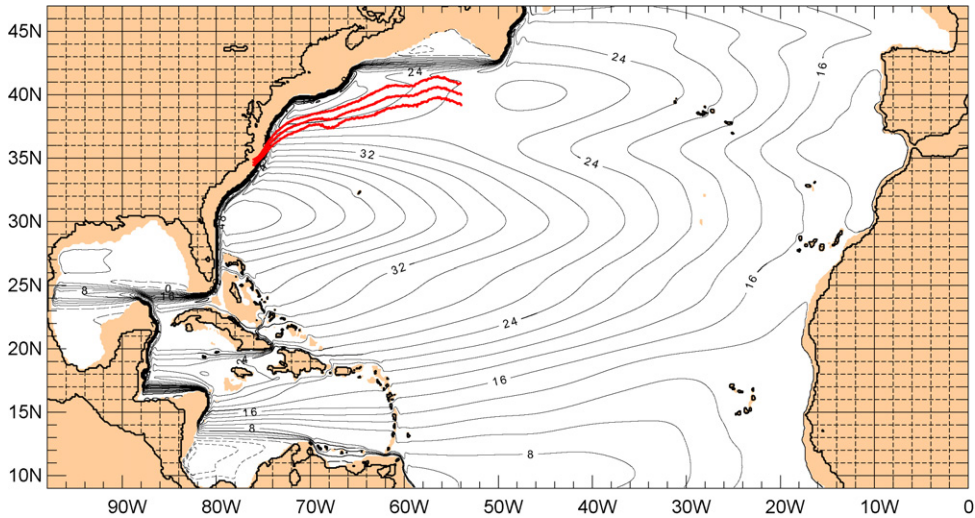


Fig. 1. Mean transport streamfunction (Ψ) from a $1/16^\circ$, 1.5-layer linear reduced-gravity simulation forced by the smoothed Hellerman and Rosenstein (1983) (HRsm) wind stress climatology (the same as used for all of the simulations in this article) plus the northward upper ocean flow (14 Sv) of the meridional overturning circulation (MOC). The mean Gulf Stream IR northwall pathway $\pm 1\sigma$ from Cornillon and Sirkes is overlaid. The contour interval is 2 Sv. The streamfunction shown above covers the $9\text{--}47^\circ\text{N}$ model domain used by all the nonlinear simulations discussed here (adapted from Townsend et al., 2000).

aimed at increased dynamical understanding of the Gulf Stream mean pathway and its separation from the western boundary. Thus, they are designed to investigate a range of physical and dynamical impacts on simulations of the Gulf Stream, including (a) linear versus nonlinear (Exp. $1/16^\circ\text{-1}$ versus the remaining simulations), (b) the impact of horizontal resolution and reduced explicit dissipation on the inertial character of the Gulf Stream and flow instabilities, (c) the strength of the eddy-driven abyssal circulation (particularly as a function of the model resolution and the bottom friction coefficient, $C_b = .002$ or $.02$), (d) the presence or absence of a DWBC, and (e) the inclusion of the bottom topography versus using a flat bottom (Exps. $1/32^\circ\text{-9a}$ and $1/32^\circ\text{-9c}$) or a reduced-gravity model (Exp. $1/32^\circ\text{-10a}$). The model experiments are designed to be as similar as possible to better isolate the impacts of their deviation from their nearest relatives and to facilitate interpretation of the results. Model experiments $1/8^\circ\text{-4b}$, $1/16^\circ\text{-2a}$, and $1/32^\circ\text{-2c}$ are experiments 8H, 16H and 32H in Hurlburt and Hogan (2000).

The model domain for the nonlinear simulations is shown in Fig. 1 and covers the North Atlantic from 9°N to 47°N , encompassing nearly all of the subtropical gyre. The model simulations with the bottom topography (BT in Table 1) use a significantly modified version of the $1/12^\circ$ ETOP05 topography (NOAA, 1986). This topography was first interpolated to the $1/16^\circ$ model grid, then modified for better agreement with detailed bathymetric charts (McManus et al., 1997), especially sill depths of straits and the location of the 200-m isobath, used as the model boundary in most locations. The $1/8^\circ$ and $1/32^\circ$ model boundaries and topography are interpolated versions from the $1/16^\circ$ model with subsequent minor modification. Before use in the models, the topographic depths at each resolution were smoothed twice using a nine-point smoother to reduce energy generation at small scales poorly resolved by the model.

A smoothed version of the Hellerman and Rosenstein (1983) wind stress climatology (HRsm) was used to force all of the simulations in Table 1, based on a comparison of $1/16^\circ$ linear 1.5-layer reduced-gravity North Atlantic simulations driven by 11 different wind stress climatologies (Townsend et al., 2000). HRsm was created using one pass of a nine-point smoother to eliminate two-grid-interval noise in the Hellerman and Rosenstein wind stress on the 2° native grid. Without this smoothing severe noise with a 4° wavelength was found in the wind stress curl when the unsmoothed winds were interpolated to the ocean model grid, resulting in some unrealistic features in the wind stress curl and

in the corresponding $1/16^\circ$ linear ocean model solution, especially in the North Atlantic subtropical gyre (Townsend et al., 2000).

The contribution of the MOC to the Gulf Stream system is included via ports in the western part of the northern and southern boundaries of the models. The location, transports and depth profiles of the specified port flows were chosen based on observations. See Hurlburt and Hogan (2000) for details. In the simulations with a DWBC (Table 1), the net transport through the northern (southern) boundary is 14 Sv (13 Sv) northward above the abyssal layer and 14 Sv (13 Sv) southward in the abyssal layer. This gives a net upward transport of 1 Sv from the abyssal layer to layers above within the model domain with uniform distribution of the upward transport. In the simulations without a DWBC, the northward upper ocean branch of the MOC is 14 Sv. The purely hydrodynamic nature of the model facilitates this approach of simply turning off the DWBC. Once the DWBC transports through the ports at 9°N and 47°N are turned off, no support for the DWBC is maintained in the model and it rapidly dissipates, as verified by results in Section 3. Since the model is purely hydrodynamic, no residual DWBC water mass characteristics remain.

3. Dynamics of Gulf Stream separation from the western boundary and its pathway to the Grand Banks

3.1. Linear model results

Based on results from a two-layer limited-area model of the Gulf Stream, Thompson and Schmitz (1989) found indications that the DWBC could play a role in realistic Gulf Stream separation from the coast at Cape Hatteras via the abyssal current steering mechanism. Here, we investigate Gulf Stream dynamics, including the relative influence of the DWBC and the eddy-driven mean abyssal circulation on Gulf Stream separation from the coast. The model configuration of Hurlburt and Hogan (2000) is ideal for this purpose because it is purely hydrodynamic and the model DWBC, specified by flow through ports in the northern and southern boundaries of the lowest layer, can be turned on and off at will without affecting the mass balance in the model. Further, it can appropriately represent the influence of linear dynamics driven by Sverdrup flow and a linearized western boundary current component driven by the northward upper ocean flow of the MOC.

Aside from the fact that horizontal friction is applied everywhere in the numerical model, the 1.5-layer linear simulation (Table 1) has a Sverdrup (1947) interior, Munk (1950) viscous western boundary layers, and it is consistent with the theory of Godfrey (1989) for including islands. The northward upper ocean flow of the MOC (14 Sv) is included via ports in the model boundaries and assumes the form of a Munk western boundary layer with some zonal connecting segments. This solution was added to the wind-driven solution by linear superposition. Mass transport streamfunction (ψ) from the combined result, using wind forcing from the HRsm wind stress climatology, is shown in Fig. 1.

The linear solution gives two Gulf Streams, (1) a broad wind-driven pathway extending eastward from the western boundary ($\sim 5^\circ$ wide centered along 35.5°N) and (2) an MOC plus second wind-driven pathway that continues northward along the western boundary except for a zonal segment at $42\text{--}43^\circ\text{N}$. From the streamfunction (ψ) in Fig. 1, the total western boundary current transport in the linear simulation is 44 Sv at 33°N near the southern edge of the broad eastward flow. Of this transport, half flows eastward into the interior (leaving the coast between 33°N and 38°N) and half continues along the western boundary (14 Sv from the MOC and 8 Sv from the wind forcing). Both pathways show poor agreement with the observed 15-year mean (1982–1996) pathway of the satellite IR northwall SST front from Cornillon and Sirkes (unpublished work, see acknowledgements). The methodology for automated determination of the frontal locations is discussed in Cayula and Cornillon (1995). An early application of IR frontal analysis to the Gulf Stream is discussed in Cornillon (1986) and an earlier analysis of the mean Gulf Stream IR northwall frontal pathway and its variability (based on data from 1982 to 1989) is discussed in Lee and Cornillon (1996). From the linear solution, it is easy to see why simulating a realistic single nonlinear Gulf Stream pathway between Cape Hatteras and the Grand Banks has been a challenging problem for ocean modelers.

3.2. Impacts of the DWBC and the eddy-driven abyssal circulation on the Gulf Stream pathway

Here we investigate the influence of the DWBC, the eddy-driven mean abyssal circulation, and the inertial character of the jet on the nonlinear Gulf Stream pathway using the same basic $1/8^\circ$, $1/16^\circ$ and $1/32^\circ$ numerical models as Hurlburt and Hogan (2000). The two studies also share a small subset of the simulations they utilize (identified in footnote 'g' of Table 1). Fig. 2 depicts the mean SSH in the region of interest from six simulations that address the topic: $1/16^\circ$ simulations (a) with and (b) without a DWBC, $1/32^\circ$ simulations (c) with and (d) without a DWBC, and $1/32^\circ$ simulations where the coefficient of quadratic bottom friction (C_b) has been increased from .002 to .02 (e) with and (f) without a DWBC. The purpose of the $10\times$ increase in C_b is to investigate the impact of greatly reducing the eddy-driven abyssal circulation on the Gulf Stream simulated by the $1/32^\circ$ model. The northward upper ocean flow of the MOC is included via ports in the northern and southern boundaries in all of the simulations and the mean IR northwall frontal pathway from Cornillon and Sirkes is overlaid on each panel. Two of the simulations, $1/16^\circ$ and $1/32^\circ$ with a DWBC (Fig. 2a and c), were also used by Hurlburt and Hogan (2000), who performed numerous model-data comparisons with these simulations.

All three of the simulations with a DWBC (Fig. 2a, c, and e) exhibit realistic Gulf Stream separation from the coast at Cape Hatteras and a generally realistic mean stream pathway between Cape Hatteras and the Grand Banks. The $1/16^\circ$ model results suggest that the DWBC is crucial for realistic Gulf Stream separation from the western boundary, because without it the simulated Gulf Stream pathway overshoots the observed separation latitude (Fig. 2b). In sharp contrast, the $1/32^\circ$ model (with $C_b = .002$) demonstrates almost no impact of the DWBC on Gulf Stream separation from the coast or any of the stream pathway depicted, except southeast of the Grand Banks. Thus, the conclusion one might draw about the impact of the DWBC on Gulf Stream separation could depend on ocean model resolution.

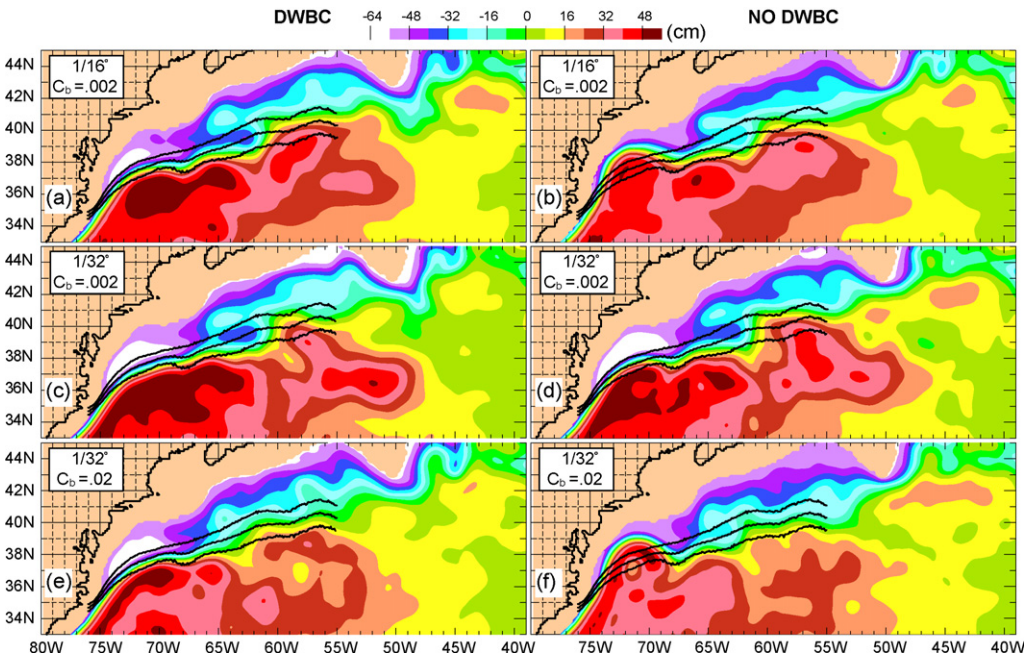


Fig. 2. Mean SSH from six 5-layer Atlantic Ocean simulations (9–47°N) including the Intra-Americas Sea zoomed into the Gulf Stream region between Cape Hatteras and the Grand Banks. The simulations depicted in (a), (c) and (e) include a DWBC while those in (b), (d) and (f) do not. (a) and (b) Depict results from $1/16^\circ$ simulations, (c–f) from corresponding $1/32^\circ$ simulations, (a–d) with a standard bottom drag coefficient of $C_b = .002$, (d) and (f) with a $10\times$ increase to $C_b = .02$. The northward upper ocean flow of the MOC is included in all six simulations. The SSH contour interval is 8 cm. The mean Gulf Stream IR northwall pathway $\pm 1\sigma$ from Cornillon and Sirkes is overlaid on each panel.

When the value of C_b is increased by $10\times$ in the $1/32^\circ$ model, the DWBC is again crucial in simulating realistic Gulf Stream separation from the western boundary (Fig. 2e versus Fig. 2f), as in the $1/16^\circ$ model.

These results suggest that if the eddy-driven mean abyssal circulation is sufficiently strong, the DWBC is not needed to obtain realistic Gulf Stream separation from the coast, but when it is weaker the DWBC can play a crucial role. Hurlburt and Hogan (2000) showed that a corresponding $1/8^\circ$ simulation gives unrealistic Gulf Stream overshoot of the observed separation latitude even with a DWBC. Thus, the DWBC is neither necessary nor sufficient in simulating realistic Gulf Stream separation from the western boundary. However, in an intermediate range of model parameter space, it can play a crucial contributing role.

The Gulf Stream transitions to the northward North Atlantic Current southeast of the Grand Banks. In the simulations with a DWBC there are two mean pathways (inner and outer meanders) where the Gulf Stream makes this transition as it rounds the southern tip of the Grand Banks (located near 43°N , 50°W) (Fig. 2a, c, and e), albeit a weak outer meander in the simulation with high bottom friction ($C_b = .02$) (Fig. 2e). This phenomenon is also seen in the $1/8^\circ$ model (Table 1), as shown in Hurlburt and Hogan (2000, their Fig. 4a). Without a DWBC, only the inner meander pathway exists (Fig. 2b, d, and f). The outer meander pathway is driven by the DWBC as it rounds the Southeast Newfoundland Ridge southeast of the Grand Banks. Both pathways are observed (Kearns and Rossby, 1998).

Near the Gulf Stream separation from the coast, all six of the simulations shown in Fig. 2 have mean maximum surface layer current speeds (see Table 2 in Section 3.4) in line with observations reported by Halkin and Rossby (1985), Joyce et al. (1986), Johns et al. (1995), and Schmitz (1996). Thus, differences in the separation pathway cannot be attributed to differences in the inertial character of the simulated currents. Based on the linear simulation (Fig. 1), a strong inertial jet is clearly essential to obtain a realistic single Gulf Stream pathway. Here, all of the simulations with a realistic separation pathway have a clearly defined cyclonic recirculation gyre on the north side of the separating current, i.e. there is no residual mean northward flow along the western boundary north of the simulated Gulf Stream separation, unlike the linear solution (Fig. 1). The simulations with Gulf Stream overshoot (Fig. 2b and f) separate from the western boundary at the same latitude as the other simulations in Fig. 2. They exhibit a very small cyclonic gyre west of the overshooting current (marked by light violet in Fig. 2b and f) that has southward flow on the western side.

The nonlinear simulations in Fig. 2 tend to exhibit a relatively stable Gulf Stream pathway between the coast and 69°W and greater meandering and ring generation farther to the east, consistent with the observed increase in the overlaid standard deviation of the Gulf Stream IR northwall frontal pathway. This pattern of increase and broadening of the variability is also seen in SSH variability from satellite altimetry and in the model simulations (see model-data comparisons for the simulations depicted in Fig. 2a and c in Hurlburt and Hogan, 2000, exps. 16H and 32H in their Fig. 9). At 68°W the observed IR northwall front depicts a slight southward dip in the Gulf Stream pathway, a dip seen in all of the simulations to varying degrees. It is also seen in the mean Gulf Stream axis from in situ data, defined as the 12°C isotherm at 400 m depth (Watts et al., 1995, their Fig. 4) and in the earlier Gulf Stream IR frontal analysis by Lee and Cornillon (1996).

To illustrate the influence of the abyssal circulation on the Gulf Stream pathway, Fig. 3 depicts the mean abyssal layer currents superimposed on their speed (in color) for the same six simulations. All of the simulations give a generally realistic mean Gulf Stream pathway east of 68°W . Thus we look for abyssal currents passing under the Gulf Stream west of that longitude for influence on its separation from the coast, starting with the $1/32^\circ$ simulation that has a DWBC and $C_b = .002$ (Fig. 3c). In this simulation there are three locations west of 68°W where generally southward currents cross under the observed and modeled Gulf Stream pathway, one between 68.5°W and 69°W , a confluence of two currents between 71°W and 73°W with the stronger branch lying between 71°W and 72°W , and a narrow third current adjacent to the model boundary near 75°W . The abyssal current just east of 69°W is present in all of the simulations but is weakest in the two simulations (Fig. 3b and f) where the model Gulf Stream pathway overshoots the observed latitude west of 68°W and is $.5\text{--}.7^\circ$ too far north at 69°W (Fig. 2b and f). The confluence of two abyssal currents ($71\text{--}73^\circ\text{W}$) is present in some form in all the simulations with a DWBC and none of the simulations without one. This flow is strongest in the $1/32^\circ$ simulation with $C_b = .002$ (Fig. 3c). In that simulation it leads to a distinct local straightening of

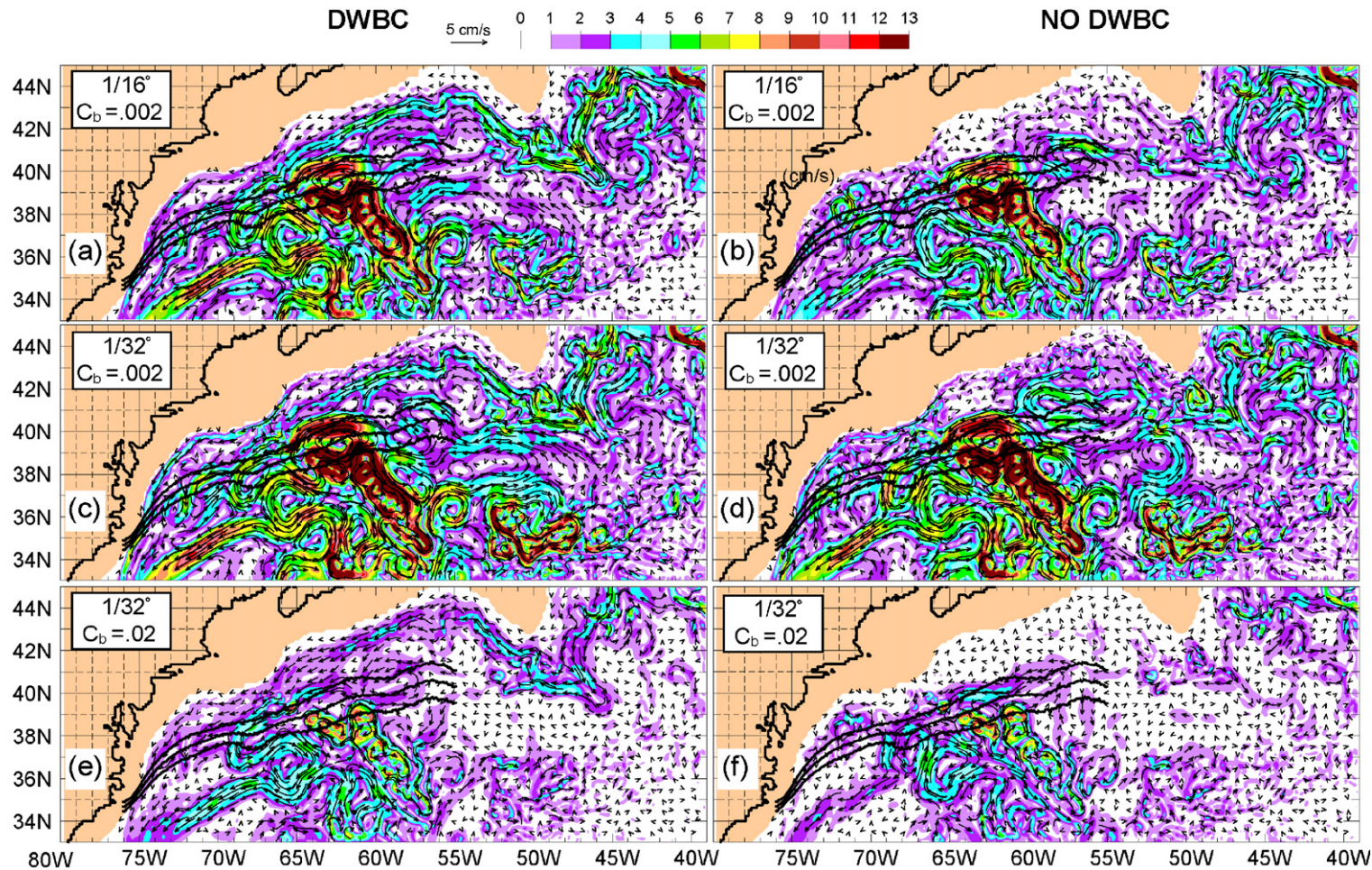


Fig. 3. Same as Fig. 2 except for mean abyssal currents (arrows) overlaid on isotachs (in cm s^{-1}). The DWBC is most easily seen paralleling the northern model boundary north of 41°N between 65°W and 51°W in panels (a, c, and e). In the simulations with no DWBC (panels b, d, and f) that current is not present.

the model Gulf Stream pathway (slight local southward depression compared to Fig. 2a, d, and e) not seen in any of the other simulations. This local straightening is consistent with the mean IR northwall pathway (Fig. 2c) and with the mean pathway at 400 m depth depicted in Watts et al. (1995). The third current adjacent to the model boundary is present in all but one of the simulations (Fig. 3f), but for each pair of simulations it is stronger in the member with a DWBC. The current that passes under the Gulf Stream axis near 38°N, 68.5°W lies above the foot of the continental slope (~4200 m isobath north of the Gulf Stream) until it separates onto the abyssal plain at ~37.5°N (Fig. 4a). This separation process begins where the foot of the continental slope shifts to a slightly shallower depth farther to the west. Part of the abyssal current continues along the foot of the continental slope (above the 3000–3900 m isobaths). The stronger (weaker) branch of this continuation is centered above the ~3600 m (3100 m) isobath north of the Gulf Stream and crosses under it at 71–72°W (72–73°W). These two branches merge beneath the stream and cross under it near 72°W (Fig. 5d).

With one exception the DWBC strengthens all three abyssal current pathways that pass under the Gulf Stream (the exception being the pathway at 68.5–69°W in the 1/32° simulations with standard bottom friction, Fig. 3c versus Fig. 3d). A 1/8° version of the model simulates almost no eddy-driven mean abyssal circulation, only a DWBC hugging the continental slope and crossing under the observed latitude of the Gulf Stream at 71–72°W (Fig. 4b and Hurlburt and Hogan, 2000, their Fig. 10a). However, in the 1/16° and 1/32° simulations shown in Figs. 3a and c and 4a, all of the DWBC contributions to the abyssal current crossing under the Gulf Stream at 68.5–69°W and part (most) of the 1/16° (1/32°) abyssal current passing under the Gulf Stream near 72°W retroflects onto the interior abyssal plain. There it joins the eddy-driven abyssal circulation where both the DWBC and the eddy-driven contributions take multiple complex pathways until emerging as a single west-southwestward abyssal current above the ~4600–5100 m isobaths near 35.5°N, 67–68°W. This current reaches the continental slope near 33°N where it rejoins the DWBC component that continued along the slope without retroflecting into the basin interior (see Hurlburt and Hogan, 2000, their Fig. 11). The latter is relatively weak in the model simulations and follows the ~3700 m isobath south of 35.5°N in Fig. 4a, ~2 cm s⁻¹ in the model versus ~3 cm s⁻¹ in the same direction from a near-bottom mean current meter measurement over the ~3800 m isobath near 35.1°N (Pickart and Watts, 1990, their Fig. 1). The existence and strength of the west-southwestward jet is corroborated by a near-bottom mean current meter measurement near 34.5°N, 71.1°W that gives a mean abyssal current in the same direction with a mean velocity of ~12.5 cm s⁻¹ (Pickart and Watts, 1990) versus 10.5 cm s⁻¹ in the 6-year model mean of Fig. 4a.

As an aside, since the relatively strong interior abyssal current that rejoins the DWBC along the continental slope near 33°N lies above deeper isobaths than the weaker branch that continues along the continental slope (Fig. 4a), unlike the DWBC in the 1/8° model (Fig. 4b) and the shallowest pathway in the higher resolution models, it never intrudes west of 75°W north of 31°N and it does not intrude under the Gulf Stream. Model DWBCs centered above a sufficiently shallow isobath can cross under the Gulf Stream as they meander eastward near 31–32°N (Fig. 4b) around the Blake Bahama Outer Ridge and could cause unrealistic Gulf Stream meandering away from the coast, a problem sometimes seen in a number of ocean models, including z-level (Smith et al., 2000), isopycnic (Chassignet and Marshall, 2008), and some of our NLOM and HYbrid Coordinate Ocean Model (HYCOM) simulations.

In an observationally based schematic diagram of abyssal thermohaline circulation pathways, Schmitz and McCartney (1993, their Fig. 12a) show a branch of the DWBC retroflecting into the interior at 38°N, 71°W as well as a branch continuing along the continental slope. All of the 1/8°, 1/16°, and 1/32° simulations with a DWBC used in Figs. 2–4 yield an abyssal current, that depends on the DWBC for its existence, passing through these coordinates. The branch continuing along the continental slope beyond the retroflexion is weak in the 1/32° simulations (Figs. 2c and 4a), but dominant in the 1/16° simulation (Fig. 2a). Schmitz and McCartney also define an entirely interior pathway originating where the DWBC rounds the southern tip of the Southeast Newfoundland Ridge. Analogous but significantly different pathways can be traced in Fig. 3a and c (stronger in 3c). Also see Figs. 10 and 11 in Hurlburt and Hogan (2000) for broader views of the pathways in Fig. 3c. Both interior pathways in the Schmitz and McCartney schematic rejoin the DWBC along the continental slope between 33°N and 35°N in a manner similar to that seen in the model simulations (Figs. 3 and 4a; Hurlburt and Hogan, 2000, Fig. 11).

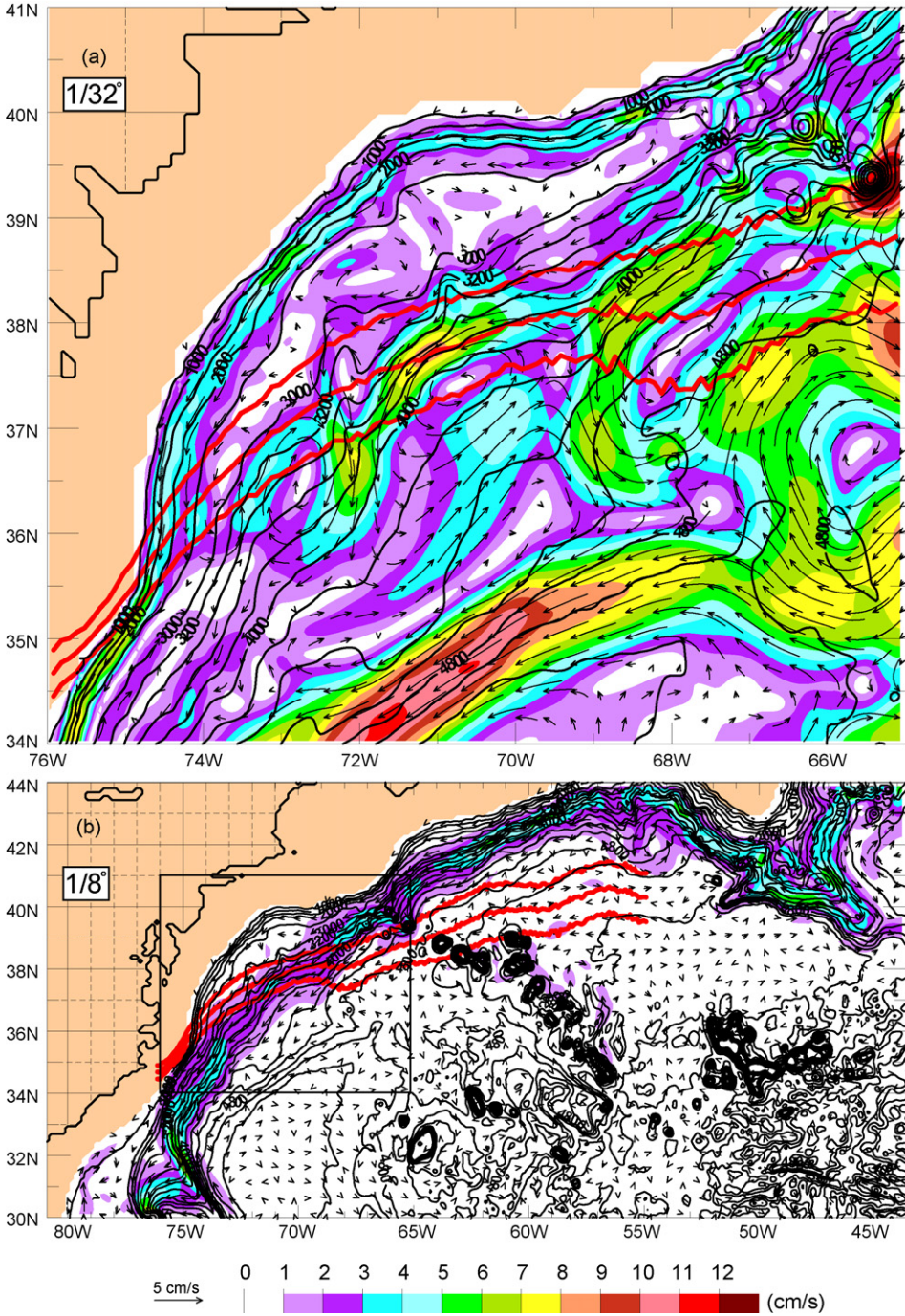


Fig. 4. (a) Zoom of Fig. 3c with (full amplitude, uncompressed) depth contours (in m) overlaid to facilitate geographical collocation of the model-data comparisons. (b) Same as (a) but for the 1/8° simulation over a larger region with a box outlining the region covered by (a).

All three of the model abyssal current pathways passing generally southward under the Gulf Stream have both an eddy-driven and a DWBC contribution (Fig. 3). Here the two simulations with the weakest support from these abyssal currents (no support from one or two of them) are the two with the unrealistic overshoot in the Gulf Stream pathway west of 68°W (Fig. 2). Of the three southward abyssal

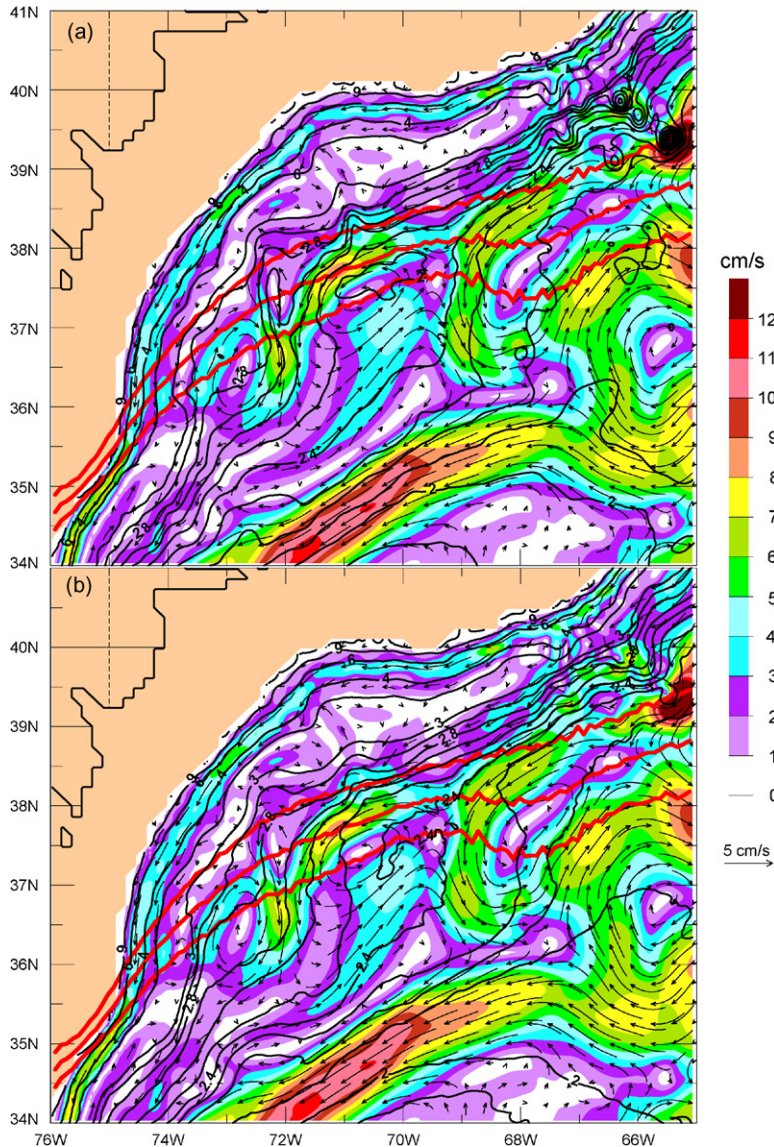


Fig. 5. (a and b) Same as Fig. 4a but with depth contours replaced by contours of (a) abyssal layer planetary potential vorticity (PPV) and (b) Eulerian mean potential vorticity (\overline{PV}) in units of $10^{-8} \text{ m}^{-1} \text{ s}^{-1}$. $PPV = f/h_5$, where f is the Coriolis parameter and \bar{h}_5 is the temporal mean thickness of the layer between the base of the thermocline and the seafloor (layer 5). $\overline{PV} = (\zeta_5 + f)/h_5$, where ζ_5 is the relative vorticity in layer 5. (c) The Eulerian mean contribution of relative vorticity to \overline{PV} , ζ_5/h_5 in units of $10^{-10} \text{ m}^{-1} \text{ s}^{-1}$ (in color) and (d) the mean depth at the base of the model thermocline (in m) from the same simulation (mean depth of the interface between layer 4 and layer 5 [the abyssal layer] in Exp. 1/32°-2c) (in color), both overlaid on mean abyssal currents and (full amplitude, uncompressed) topographic contours.

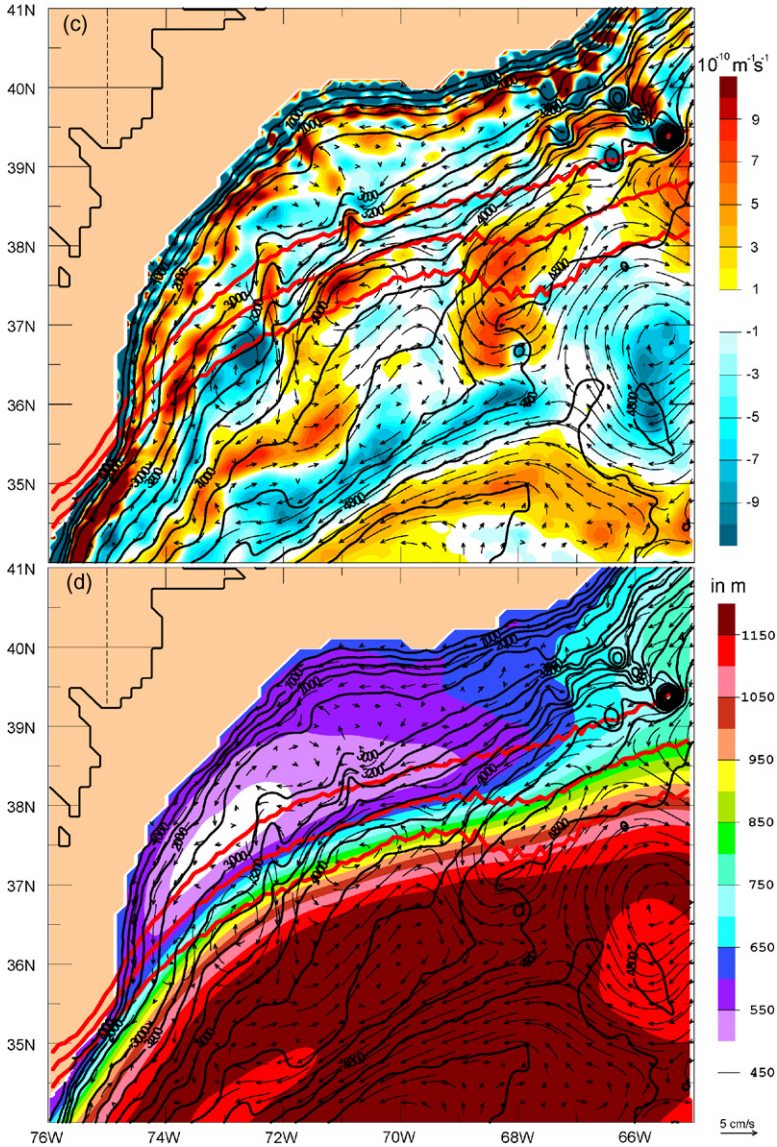


Fig. 5. (Continued).

currents, the one at 68.5–69°W has the greatest impact, an impact analogous to that of an unrealistic southward abyssal current on the Loop Current in a Gulf of Mexico simulation discussed in Hurlburt and Thompson (1980) and Hurlburt et al. (2008). The confluent pathway (71–73°W) does not exist in the simulations without a DWBC. Thus, it is not essential in the 1/32° model with $C_b = .002$ even though it has some impact, as discussed earlier. Further investigation is needed to see if it is essential in the model simulations requiring a DWBC contribution, but no local response to it is evident. No impact on the Gulf Stream pathway was discerned from the third abyssal current, the narrow current along the model western boundary, consistent with observations (Pickart, 1994). Pickart (1994) finds only a 14° mean angle between this southwestward abyssal current and the northeastward flow of

the Gulf Stream where they intersect. A similarly small angle is seen in the model simulations shown in Figs. 2 and 3, resulting in very weak steering of the Gulf Stream pathway by this abyssal current. Pickart (1994) and simulation 1/32°-2c (Fig. 4a) both give mean speeds of $\sim 5 \text{ cm s}^{-1}$ for the abyssal current where it crosses under the Gulf Stream.

3.3. Gulf Stream impact on abyssal current potential vorticity and resulting feedback affecting the Gulf Stream pathway

The main focus of the previous section was abyssal circulation impacts on the Gulf Stream pathway between its separation from the western boundary and $\sim 68^\circ\text{W}$. In this section we address Gulf Stream impacts on the abyssal circulation from a potential vorticity point of view and a resulting feedback that influences its pathway. Hogg and Stommel (1985) noted that the DWBC followed the $3400 \pm 200 \text{ m}$ isobath north of the Gulf Stream and the $4200 \pm 200 \text{ m}$ isobath south of it. Using a steady two-layer model they showed that the DWBC could pass under the Gulf Stream and conserve potential vorticity by crossing isobaths to greater depths, a theory first corroborated by observational evidence presented by Pickart and Watts (1990). In observations, the base of the thermocline typically increases in depth by about 700–800 m from north to south across the Gulf Stream (e.g. Joyce et al., 1986; Bower and Hunt, 2000a) and it increases by $\sim 600 \text{ m}$ in the model simulations between the western boundary and 69°W (Fig. 5d). It is now known that the DWBC transports four distinct water masses over a depth range of 700–4000 m (Bower and Hunt, 2000a). Here we consider only the deeper DWBC pathways as the shallower pathway crossing under the Gulf Stream near 75°W had no significant impact on the mean Gulf Stream pathway in observations (Pickart, 1994) or the model.

There are three mean abyssal current pathways in the model that cross generally southward under the Gulf Stream between 73°W and 68°W . These cross at $68.5\text{--}69^\circ\text{W}$, $71\text{--}72^\circ\text{W}$ and $72\text{--}73^\circ\text{W}$. The last two are confluent currents near 72°W beneath the model Gulf Stream (Fig. 5d) and then separate again near 36°N with the western branch continuing along the continental slope and the eastern one retroflecting into the interior (Fig. 4a). Even though the two western cross-under pathways have an eddy-driven contribution, they do not exist in the simulations without a DWBC, as discussed earlier. The westernmost of the three pathways follows the $\sim 3100 \text{ m}$ isobath north of the Gulf Stream and the $\sim 3700 \text{ m}$ isobath south of the stream. All three cross isobaths to deeper depths by $\sim 600 \text{ m}$ while crossing under the model Gulf Stream (Fig. 5d).

Bower and Hunt (2000a,b) discuss results from a 2-year RAFOS float deployment at ~ 1000 and $\sim 3000\text{-dbar}$, the latter mostly between the 3500 and 4000 m isobaths. Here we consider only their results from the 14 floats at $\sim 3000\text{-dbar}$, since they are very useful in the evaluation and interpretation of abyssal layer model results. The float trajectories can be divided into two basic groups, those that cross under the Gulf Stream surface front east of $\sim 71^\circ\text{W}$ and mostly retroflect eastward into the basin interior south of the Gulf Stream and those that cross under west of $\sim 71^\circ\text{W}$ and mostly proceed southwestward along the deep continental slope. The RAFOS float trajectories tend to show evidence of abyssal current eddies, including floats crossing under the Gulf Stream surface front near 72°W that show some evidence of eastward or northward retroflection south of the stream (see Bower and Hunt, 2000b, their Fig. 7). The eddying trajectories are consistent with high abyssal current eddy kinetic energy (EKE) in this region seen in current meter data (Schmitz, 1996) and the model simulations (Hurlburt and Hogan, 2000, their Fig. 12).

Despite the eddy activity, the RAFOS float trajectories are remarkably consistent with the mean abyssal flow in the model, some in detail, e.g. Bower and Hunt's Fig. 7d (trajectory for float #281) and 7j (float #262). Float #281 closely follows a model mean abyssal current that passes under the Gulf Stream surface front just east of 72°W , including a slight eastward meander in the current toward deeper isobaths ($\sim 4000 \text{ m}$) on the south side of the stream ($36\text{--}37^\circ\text{N}$) before resuming a DWBC pathway over a slightly shallower isobath ($\sim 3700 \text{ m}$). Float #262 crosses under the Gulf Stream near 69°W and, with some eddying motion along the trajectory, takes a short retroflection pathway for a float crossing under the Gulf Stream at that longitude, i.e., an eastward retroflection near 37°N , 70°W followed by a westward retroflection near 36°N , 68°W . After the second retroflection, the float returns toward the western continental slope above the 4800 m isobath. The trajectory of float #262 is consistent with the model mean abyssal circulation (Fig. 4a) plus some eddy motions. The final leg of the trajectory lies

along the northern part of a gentle escarpment seen in Fig. 4a and b. This escarpment constrains the pathway of the main conduit by which abyssal flow in the model simulations (Fig. 3) (emerging from any interior pathway) returns to the western continental slope near 33°N (see Hurlburt and Hogan, 2000, their Fig. 11). That includes a major portion of the DWBC, as can be seen by comparing the strength this abyssal current in the corresponding simulations with and without a DWBC in Fig. 3. Most of the other floats crossing under the Gulf Stream surface front east of 71°W retroreflect much farther into the basin interior than #262 south of the Gulf Stream, again consistent with the model mean abyssal flow.

Bower and Hunt (2000a, their Fig. 12) and Bower and Hunt (2000b, their Fig. 17) present maps of planetary potential vorticity (PPV), i.e. f/h_a , where h_a is the climatological mean thickness of the abyssal layer between the main thermocline and the seafloor. These maps depict ridges of relatively high PPV south of the Gulf Stream consistent with the retroreflections exhibited by the trajectories of deep RAFOS floats and the model mean abyssal currents in that area. However, the model PPV (f/\bar{h}_5 , where \bar{h}_5 is the temporal mean thickness of the model abyssal layer) does not depict a significant ridge south of the Gulf Stream (Fig. 5a). Instead, it shows a weak zonal PPV gradient with lower values toward the east and with the mean abyssal currents retroreflecting into the basin interior while crossing these weak gradients toward lower PPV. Thus mean PPV is not sufficient to explain the preceding retroreflections. Additional effects on potential vorticity (PV) such as relative vorticity, temporal variations in abyssal layer thickness, abyssal current dissipation and diapycnal mixing need to be considered. Model mean PPV and Eulerian mean PV give similar results (Fig. 5). While the differences are generally modest, the anticyclonic flow around the New England seamounts decreases mean PV relative to mean PPV by up to 1/3, largely erasing the mean PPV signature of the seamounts located in the northeast corner of each figure panel. Since conservation of PV is a Lagrangian property of the flow, a model study of the abyssal circulation in a Lagrangian framework, considering a wider range of effects on PV, would be an interesting topic for future research. Bower and Hunt (2000b) calculated PV along the tracks of two deep RAFOS floats and found it decreased slowly with time.

Model mean abyssal currents do follow PPV contours quite well over most steeper slopes, including the locations where the mean abyssal currents cross under the mean Gulf Stream (Fig. 5a and d). In these areas the mean abyssal currents passing under the Gulf Stream cross topographic contours to deeper depths much more than they cross mean PPV or PV contours (Fig. 5). A preferred location for mean abyssal gyres is found directly beneath the mean Gulf Stream because the base of the Gulf Stream thermocline (interface between layers 4 and 5 in the model) typically allows currents to go deeper when southward and shallower when northward, thus permitting a region of relatively uniform PV above the sloping topography. A series of four mean abyssal gyres are simulated beneath the Gulf Stream between 74°W and 67°W (Fig. 5d), three cyclonic and one anticyclonic, the westernmost only ~0.5° in diameter centered near 73.8°W, 36.2°N. The cyclonic mean gyre centered near 70.8°W, 37.4°N in the model is clearly outlined in the means from eight near-bottom current meter moorings that yielded mean speeds and directions similar to the model (Pickart and Watts, 1990, their Fig. 1). Additionally, the model mean gyre centered near 68°W, 37.8°N is supported by 26-month means from an array of 15 current meter moorings at 3500 m depth, again with similar mean speeds (Johns et al., 1995, their Fig. 2). In each case the gyre boundary with a southward component and stronger currents (in some cases augmented by the DWBC) tends to be determined by relatively steep topographic slopes as are the pathways of the abyssal currents feeding into the mean gyres on the northside. The latter exit the gyres on the south side mostly as eastward currents retroreflecting onto the abyssal plain, but with the westernmost branch continuing southward along the continental slope. The westernmost retroreflection occurs near 72°W, consistent with the ~3000-dbar RAFOS float trajectories presented by Bower and Hunt (2000b).

One might anticipate a tendency to generate positive relative vorticity (ζ_5) due to some vortex stretching as the generally southward abyssal currents flow toward deeper depths under the Gulf Stream. While positive ζ_5 is generated in the three examples where a cyclonic mean abyssal gyre is simulated beneath the Gulf Stream, in one example negative ζ_5 and an anticyclonic gyre are generated (centered near 36.5°N, 72.7°W) (Fig. 5c). Upon examination, it is evident that the sign of the relative vorticity is largely determined by constraints of the topographic configuration as the abyssal current

crosses to deeper depths, i.e. whether the topography requires curvature toward the east or the west as the abyssal current crosses under the stream.

In Section 3.2 we discussed effects of abyssal current steering on the mean path of the Gulf Stream and in this section effects of the Gulf Stream on abyssal current pathways, but what determines the mean latitude of the Gulf Stream where the mean abyssal currents cross under? Based on the two-layer theory presented in Section 2, further abyssal current advection of the upper ocean current pathway would cease in the mean when a mean balance occurred between advection and primarily divergence in the continuity equation, likely assisted by a decrease in abyssal current steering, a decrease to zero in the case where the upper ocean and abyssal currents become parallel or antiparallel. It is particularly worthy of note that the mean abyssal currents at $68.5\text{--}69^\circ\text{W}$ and $71\text{--}73^\circ\text{W}$ pass under the Gulf Stream where the isobaths they are following diverge and accordingly the steepness of the slopes decreases (Fig. 4a). Observationally, this behavior is illustrated at 3500 m depth in Fig. 2 of Johns et al. (1995) for the abyssal current cross-under at $68\text{--}69^\circ\text{W}$. These results suggest that the termini of steeper escarpments associated with the continental slope help determine the latitude of the Gulf Stream pathway at $68.5\text{--}69^\circ\text{W}$ and $71\text{--}73^\circ\text{W}$. They do this by determining the latitude where the abyssal current can develop positive relative vorticity and retroflect eastward onto the abyssal plain after it passes under the Gulf Stream as a consequence of crossing to deeper isobaths and conserving potential vorticity during its passage under the stream. The eastward retroflection then halts further southward advection of the Gulf Stream pathway. In one case negative vorticity and curvature toward the west is generated, but with similar effect. Thus Gulf Stream impacts on the abyssal currents provide feedbacks that in turn help determine the pathway of the stream.

3.4. *Gulf Stream pathway as an inertial jet following a CAV trajectory from boundary separation to $\sim 70^\circ\text{W}$*

In Section 3.3 we discussed a constraint on the latitude of the Gulf Stream pathway at $68.5\text{--}69^\circ\text{W}$ and we showed that the existence of the constraint depended on the strength of a key abyssal current as it crossed under the Gulf Stream. Further, the simulated Gulf Stream pathways between the western boundary and 69°W agreed closely with the observed IR pathway when the latitudinal constraint at $68.5\text{--}69^\circ\text{W}$ was present, but it overshot the observed latitude of the Gulf Stream when it was absent, making the key abyssal current crucial to Gulf Stream separation in the simulations. The simulated Gulf Stream pathways exhibit low sensitivity to abyssal currents passing under the Gulf Stream west of 69°W , a pair of confluent currents at $71\text{--}73^\circ\text{W}$ (depending on the DWBC for their existence) and a current along the western boundary near 75°W . The reason for low sensitivity to the current at 75°W was explained at the end of Section 3.2. A constraint similar to that at $68.5\text{--}69^\circ\text{W}$ was used to explain the latitude of the Gulf Stream at $71\text{--}73^\circ\text{W}$ and the impact of the DWBC on one simulation (Exp. 1/32°-2c, Figs. 2c, 3c, 4a and 5), as evidenced by the localized straightening of the pathway compared to the more rounded curve of the other realistically simulated Gulf Stream pathways, where evidence for the same explanation is lacking. Even for Exp. 1/32°-2c the preceding effect is a small perturbation to an inertial jet, which overall exhibits close agreement with the three other simulations that have a realistic Gulf Stream pathway between the western boundary and 68°W , including Exp. 1/32°-2d (Figs. 2d and 3d) that has no DWBC, but is otherwise identical in design to Exp. 1/32°-2c (Table 1). Constraint of the Gulf Stream latitude over one small longitude interval ($68.5\text{--}69^\circ\text{W}$) is not a sufficient explanation of the Gulf Stream pathway from the western boundary to 69°W . Thus there must be another essential contribution to Gulf Stream pathway dynamics over that longitude range.

Although theories for Gulf Stream separation from the western boundary abound (Dengg et al., 1996; Chassignet and Marshall, 2008), some studies have found that the coastline geometry in the region of Cape Hatteras and a strong inertial jet are important factors (Dengg, 1993; Özgökmen et al., 1997). Here we test the relevance of a particular type of inertial jet dynamics. Since all of the simulations in Fig. 2 with the same resolution have similar mean velocity as they separate from the coast and a relatively stable pathway segment between separation from the coast and 69°W , one might anticipate that they would exhibit similar constant absolute vorticity (CAV)-like pathways over that

segment, determined by the angle of separation from the coast, but only if the Gulf Stream were a free jet not influenced by the linear solution (Fig. 1). [Rossby (1940), Haltiner and Martin (1957), Reid (1972), and Hurlburt and Thompson (1980, 1982) are some references where discussions of CAV trajectories can be found.] However, in Fig. 2 that is clearly not the case as evidenced by the two simulations (Fig. 2b and f) with (a) the unrealistic Gulf Stream overshoot of the observed separation latitude from the western boundary and (b) an inflection point in the simulated Gulf Stream pathway near 36.75°N , 74°W which is not permissible at that location, if the Gulf Stream separated from the western boundary as a free jet following a CAV trajectory. Therefore, it is not possible to explain the simulated Gulf Stream pathways between the western boundary and 69°W in Fig. 2 using CAV trajectories alone. Still, there is no inflection point within that pathway segment in the observed IR northwall (Fig. 4a) or in the four simulations with realistic separation from the western boundary (Fig. 2).

In the linear simulation (Fig. 1), half of the Gulf Stream transport continues to hug the western boundary north of the observed separation latitude. Clearly, the nonlinear Gulf Stream simulations in Fig. 2 were not sufficiently inertial to overcome the constraints of the linear solution and effect realistic Gulf Stream separation from the coast without assistance from the abyssal circulation, even though the models simulated realistic velocities at the core of the current, as it separated from the coast, in all six of the simulations. Here we investigate the possibility that the four simulations in Fig. 2 with realistic Gulf Stream pathways were able to simulate a nearly CAV trajectory between the western boundary and 69°W with assistance from the abyssal current passing under the Gulf Stream at $68.5\text{--}69^{\circ}\text{W}$. Thus we test the hypothesis that together CAV trajectories and the abyssal constraint on the Gulf Stream latitude at $68.5\text{--}69^{\circ}\text{W}$ can be used in explaining the Gulf Stream pathway between the western boundary and $\sim 68^{\circ}\text{W}$, while each alone is insufficient.

In a nonlinear 1.5 layer reduced-gravity model, a CAV trajectory requires a frictionless steady free jet with the streamline at the core of the current following contours of constant SSH and layer thickness. The latter requires a geostrophic balance so that conservation of potential vorticity becomes conservation of absolute vorticity along a streamline at the core of the current. The simulations in Fig. 2 were tested to see if the core of the current in layer 1 overlaid an SSH contour and had a narrow band of high SSH variability along the core of the current between the western boundary and 69°W , as discussed shortly.

Following Reid (1972) and Hurlburt and Thompson (1980, 1982), the CAV trajectories were calculated from:

$$\cos \alpha = \cos \alpha_0 + \frac{1}{2}y^2/r^2 - \frac{y}{\gamma_0} \quad (5)$$

which is an integrated form of the differential equation that assumes the velocity, v_c , at the core of the current is a constant, and where $r = (v_c/\beta)^{1/2}$, β is the variation of the Coriolis parameter with latitude, α is the angle of the current with respect to the positive x -axis on a β -plane, y is the distance of the trajectory from the x -axis, γ is the trajectory radius of curvature, and the subscript 0 indicates values at the origin of the trajectory calculation (here at an inflection point where $\gamma_0 \rightarrow \infty$). The amplitude (b) (here the northernmost point) of the trajectory in relation to the inflection points can be calculated from:

$$b = 2r \sin \frac{1}{2}\alpha_0 \quad (6)$$

See the references for more information about CAV trajectories.

The results of the CAV trajectory analysis are given in Fig. 6 and Table 2 for all six of the simulations shown in Fig. 2. The four simulations with a realistic Gulf Stream pathway (Fig. 6a, c, d and e) all demonstrate close agreement among the corresponding CAV trajectory (red line), the pathway of the maximum velocity at the core of the current (black line) and the SSH contour closest to the core of the current (yellow-green line) from the inflection point (marked by a red circle) where the current separates from the western boundary to $\sim 70^{\circ}\text{W}$. All four separate from the western boundary over a narrow range of angles ($53 \pm 3^{\circ}$, Table 2), guided by the angle of the boundary prior to separation. All six of the simulations show a relatively narrow band of high SSH variability along the core of the current west of 69°W and broader variability to the east in accord with the standard deviation of

Table 2
CAV trajectory analysis of simulated Gulf Stream pathways east of the western boundary

Exp. #	v_c at separation (m s^{-1})	Mean v_c over 75–70°W	α_0 wrt to x -axis, θ (°)	r (km)	b_{CAV} (km)	b_{model} wrt Lat. of α_0	b_{model} north of 35.5°N	CAV inflection point for $\alpha_0, \theta, \emptyset$	\emptyset of b_{CAV}	\emptyset of b_{model}
1/16°-2a	1.70	1.39	54.62	276	253	257	257	35.5°N, 74.55°W	70.6°W	69.9°W
1/32°-2c	2.02	1.58	53.14	294	263	263	263	35.5°N, 74.6°W	70.3°W	70.3°W
1/32°-2e	1.93	1.59	50.10	295	250	271	271	35.5°N, 74.5°W	70.1°W	69.5°W
1/16°-2b	1.55	1.21	76.07	259	319	262	389	36.7°N, 74.1°W	71.1°W	70.7°W
1/32°-2d	2.02	1.62	55.40	298	277	286	286	35.5°N, 74.65°W	70.4°W	70.0°W
1/32°-2f	1.95	1.57	72.01	295	347	261	403	36.8°N, 74.0°W	70.4°W	71.0°W

where: $r = (v_c/\beta)^{1/2}$ and v_c = speed at the core of the current, here mean v_c over 75–70°W, $\beta = 2\omega \cos \theta / r_E$, ω is the Earth's rotation rate, r_E is the radius of the earth, and θ = latitude, here 36.8°N or 38°N (the latter for the two most northern pathways).

$b_{\text{CAV}} = 2r \sin 0.5\alpha_0$ and α_0 = angle of v_c counterclockwise from eastward at the inflection point of the constant absolute vorticity (CAV) trajectory. b_{CAV} is the amplitude of the CAV trajectory with respect to (wrt) the inflection point, which should be compared to the amplitude of the model Gulf Stream pathway (b_{model} wrt the latitude of α_0). b_{model} north of 35.5°N is the maximum distance of the model Gulf Stream axis north of 35.5°N (the latitude of model Gulf Stream separation from the western boundary) between the separation point and 68.5°W. \emptyset of b_{CAV} and \emptyset of b_{model} are the longitudes at which b_{CAV} and b_{model} occur.

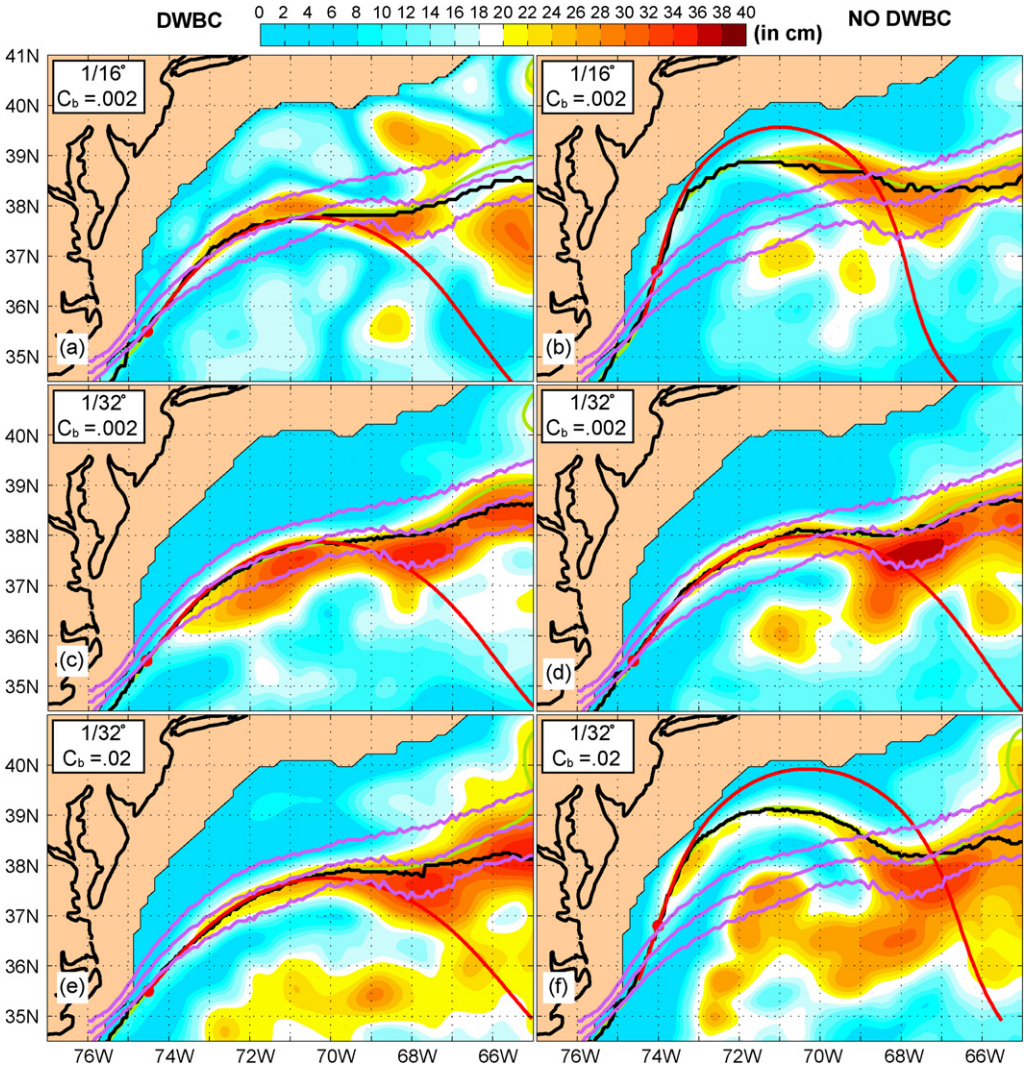


Fig. 6. CAV trajectory analysis for Gulf Stream pathways from the six simulations illustrated in Fig. 2. The pathway of the maximum velocity at the core of the current (black line), the closest SSH contour (yellow-green line), the corresponding CAV trajectory (red line with a circle at the inflection point), the observed IR northwall frontal pathway \pm S.D. (violet lines), and the simulated SSH variability are overlaid on each panel. Due to the hierarchy of the overlaid lines (light violet, red, black, yellow-green from top to bottom), lines on the bottom tend to be obscured where close agreement occurs. That is particularly the case for the yellow-green SSH contour west of $\sim 68^\circ$ W, where the core of the current overlaying a single SSH contour is a prerequisite for the existence of a CAV trajectory. The SSH contour closest to the pathway of the velocity maximum is skewed toward the north side of the modeled Gulf Stream as depicted in SSH and is (a) -24 cm, (b) -16 cm, (c) -28 cm, and (d-f) -24 cm. See the corresponding panels in Fig. 2. Near the western boundary the Gulf Stream axis from Topex/Poseidon altimetry (Lee, 1997) diverges from the IR frontal pathway in accord with the model simulations of panels a,c,d, and e (see Hurlburt and Hogan, 2000, their Fig. 7).

the IR northwall frontal pathway and along-track SSH variability from satellite altimetry (Fig. 7). The close correspondence between the CAV trajectories and mean current pathways between the western boundary and 70° W in four of the simulations demonstrates the lack of perturbations in the pathways caused by abyssal currents crossing under the Gulf Stream in that longitude range, the largest exception

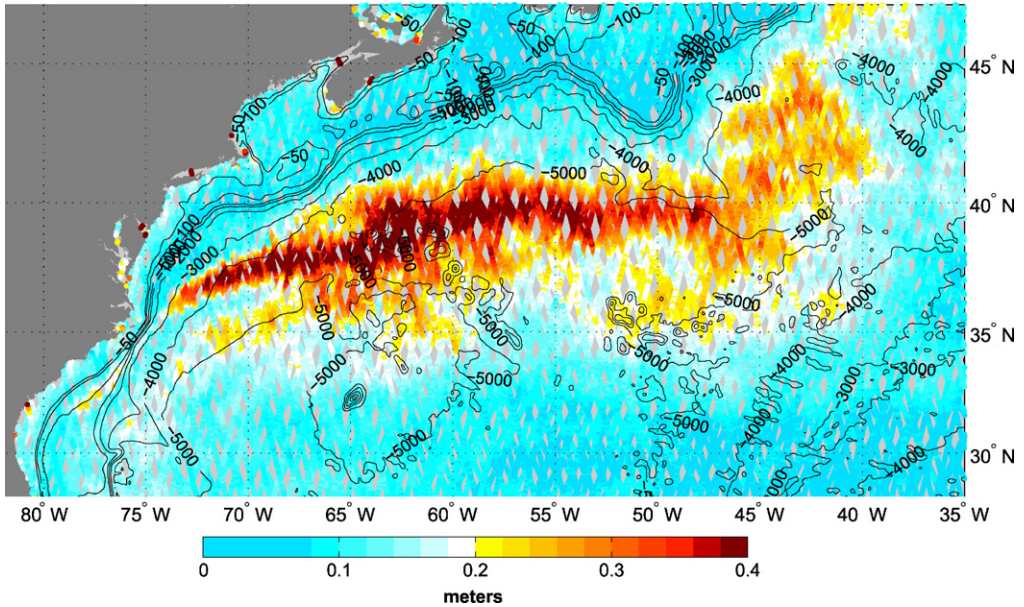


Fig. 7. Along-track SSH variability from satellite altimeter data in four different orbits overlaid on topographic contours (depth in m), Jason-1 over the period 15 January 2002 to 18 October 2007, GFO over 15 July 1999 to 12 December 2007, Envisat over 24 September 2002 to 29 October 2007, and Topex in an interleaved orbit over 16 September 2002 to 8 October 2005. The tracks are overlaid in the following order from top to bottom: (1) Envisat, (2) GFO, (3) Jason-1, and (4) Topex interleaved. (Provided by Gregg Jacobs, NRL.)

being a small southward perturbation ($\sim 1^\circ$), straightening of the pathway, and broader high SSH variability along the south side of the Gulf Stream in the $1/32^\circ$ simulation with a DWBC and $C_b = .002$ (Exp. $1/32^\circ$ -2c). These effects occur where model abyssal currents cross under the Gulf Stream. They are consistent with the IR northwall frontal pathway, which shows similar straightening of the pathway and a local increase in its standard deviation. Overall, the pathways in the four realistic simulations agree closely, and the range of variation in the northernmost point in the pathway between the western boundary and 68.5°W is only $\sim 1/4^\circ$ (b_{model} in Table 2).

Two simulations overshoot the latitude of the observed Gulf Stream pathway between the western boundary and 69°W and exhibit an inflection point in the pathway (circled on the CAV trajectory) northeast of the point where they separate from the western boundary. The model pathway and the CAV trajectory agree until the northward extent of the model pathway is limited by the northwestern model boundary. The model pathway continues to exhibit characteristics consistent with CAV dynamics (described earlier) eastward to 69°W and may follow a CAV trajectory reinitialized near 73°W with a nonzero curvature term in Eq. (5) (not tested). Because of the inflection point after pathway separation from the western boundary, these Gulf Stream simulations do not separate from the western boundary as free jets and they indicate strong influence from constraints of linear dynamics (Fig. 1), thus illustrating the need for the cooperative interaction between the influence of the abyssal current crossing under the Gulf Stream at 68.5 – 69°W and CAV dynamics in simulating a realistic Gulf Stream pathway between the western boundary and $\sim 69^\circ\text{W}$.

3.5. Gulf Stream pathway east of 68°W

Between 68°W and just west of the southern tip of the Grand Banks all six of the simulations in Fig. 2 yield generally similar and generally realistic mean Gulf Stream pathways, starting with a southward dip at 68°W . This dip is evident in the observed IR northwall frontal pathway, the mean pathway at 400 m depth from in situ data (Watts et al., 1995), and in all of the simulations depicted in Fig. 2. On

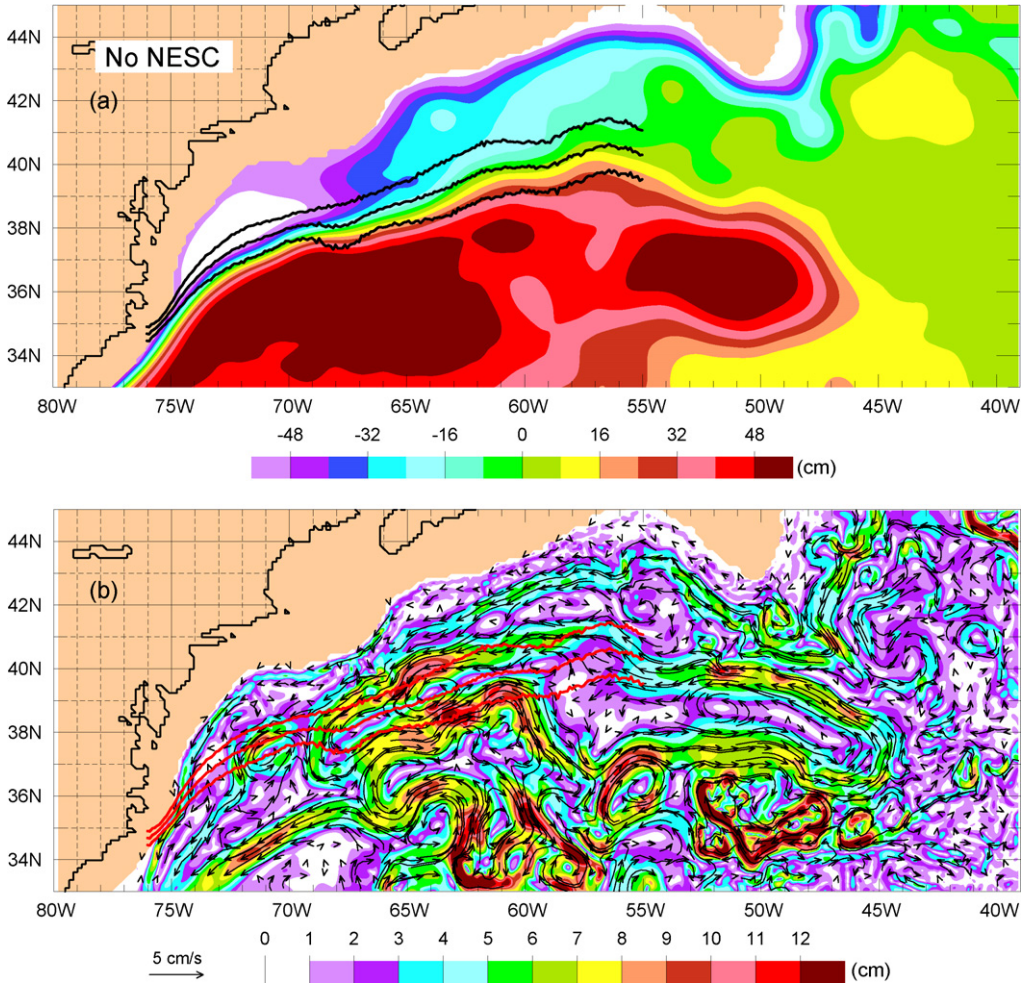


Fig. 8. Same as the $1/32^\circ$ simulation with a DWBC in (a) Fig. 2c and (b) Fig. 3c but with the New England Seamount Chain (NESC) removed.

the east side of the dip, the Gulf Stream latitude increases in the simulated and IR northwall pathways following a route above the northern edge of a simulated anticyclonic abyssal gyre (Figs. 2, 3 and 4a).

Particularly strong anticyclonic mean abyssal flow is simulated around the seamounts of the New England Seamount Chain (NESC) (Fig. 3), which extend southeastward from 40°N , 66°W to 35°N , 57°W (Figs. 4b and 7). From 38°N to 39°N the NESC forks into a “Y” which extends from 61°W to 64°W . In all but the simulations with $C_b = .02$, there is a strong mean cyclonic abyssal gyre nestled in the cup of the “Y”. These features have a significant impact on the simulated mean pathway and variability of the Gulf Stream. The simulations with the cyclonic abyssal gyre (Fig. 3a–d) give a Gulf Stream pathway that is slightly south of the IR frontal pathway along the south side of the abyssal gyre. On the east side of this abyssal gyre, northward flow steers the Gulf Stream pathway to the north. The preceding effects are reduced in the simulations with strong bottom friction (Fig. 2e and f) and in a $1/64^\circ$ simulation that is more strongly inertial east of 65°W (Hurlburt and Hogan, 2000, their Fig. 7). The effects are completely eliminated in a simulation with the NESC removed (Fig. 8a) and the cyclonic abyssal gyre extends much farther eastward and westward, from 45°W to 69°W (Fig. 8b).

As a consequence of removing the NESC, the simulated mean Gulf Stream pathway is in much better agreement with the mean IR frontal pathway from $\sim 65^\circ\text{W}$ to 55°W , but it has the most unrealistic connection between the Gulf Stream and the North Atlantic Current in comparison to Fig. 2. However, there is some disagreement between sources of observational evidence for the mean Gulf Stream pathway from about 65°W to 60°W . In this longitude band the mean pathway from satellite IR depicts a gradual increase in latitude, while the altimetry in Fig. 7 indicates a more abrupt increase near 62°W , based on the assumption that the latitudinal increase occurs toward the eastern side of the associated high variability because warm core rings shed from the Gulf Stream propagate westward from the region where the northward shift occurs. The SSH variability in Fig. 7 is derived from an average of ~ 5 years of recent quasi-contemporaneous data along altimeter tracks from satellites in four different repeat orbits. As a result it shows specific features more clearly than optimum interpolation (OI) analyses of SSH variability from one satellite (e.g. Fig. 9f of Hurlburt and Hogan, 2000), including a rather abrupt northward shift of the Gulf Stream latitude near 62°W , a phenomenon seen in the simulations with an NESC (Fig. 2). In a map of SSH variability derived from altimetry over the period 1992–2008 (not shown) some of the features seen in Fig. 7 are more blurred, including features near the NESC, and one might expect a mean Gulf Stream pathway along the axis of high variability from 65°W to 60°W and a more gradual increase in latitude, as in the IR pathway. See Hurlburt and Hogan (2000, their Fig. 9f) for a comparison between a Gulf Stream axis with coarse along-track resolution (Lee, 1997) and an OI map of SSH variability, both derived from Topex/Poseidon altimetry. In that comparison the Gulf Stream axis lies along the axis of SSH variability west of the NESC, but slightly to the north of it east of the NESC. The resolution is too coarse to define a clear pathway across the NESC.

Based on analyses of satellite IR imagery, Auer (1987) found the maximum formation rate for warm core rings occurs on the north side of the Gulf Stream near the NESC ($62\text{--}65^\circ\text{W}$), as in the model simulations (Hurlburt and Hogan, 2000). A signature of this warm core ring generation is seen in the mean SSH fields of the simulations in Fig. 2, less so in the simulation with the NESC removed (Fig. 8a). Hurlburt and Hogan (2000, their Table 5) compared the simulations in Fig. 2a ($1/16^\circ$), Fig. 2c ($1/32^\circ$) and a $1/64^\circ$ simulation with results from Auer (1987) for warm core rings north of the Gulf Stream in terms of mean population at one time, rings generated per year, and mean ring diameter. The $1/32^\circ$ and $1/64^\circ$ simulations demonstrated very good agreement in all three comparisons. Thus the altimetry and the warm core ring analysis tend to support a more abrupt northward shift in the Gulf Stream pathway (near 62°W) than depicted in the 15-year mean IR northwall pathway.

In all of the simulations shown in Fig. 2 secondary mean dips, troughs, or meanders are seen on the south side of the model Gulf Stream at one or more locations between 58°W and 64°W , e.g. the well-defined meander extending southeastward from 60°W in Fig. 2c. This mean meander is driven by southeastward flow along the east side of the NESC, consistent with the southward tongue of high SSH variability that lies just east of the NESC in Fig. 7. Mean southward dips, troughs, and meanders just west of 60°W are associated with anticyclonic mean abyssal flow around part of the western branch of the “Y”, where a second southward tongue of high SSH variability in the altimetry lies just west of the NESC. Fig. 2d shows both mean troughs in SSH. These features are preferred regions of cyclonic ring formation and southward tongues of high SSH variability, both modeled and observed (Fig. 7 and Hurlburt and Hogan, 2000, their Fig. 9). As expected, these features are removed when the NESC is removed, but a southward bulge in SSH variability similar to observations (not shown) remains, since this region still lies at the eastern end of the western nonlinear recirculation gyre (Fig. 8a). However, the southward dip at 68°W in the IR front is weaker than in any of the simulations depicted in Fig. 2 and it is shifted slightly eastward, indicating some influence of the NESC on the dip. In the simulation with no NESC, part of the abyssal gyre impinging on the Gulf Stream southeast of the dip lies slightly farther to the southeast.

4. Flat bottom and reduced-gravity simulations of the Gulf Stream

To further investigate the effects of bottom topography and the mean abyssal circulation on simulations of the Gulf Stream, we examine results from simulations with a flat bottom and a reduced-gravity simulation with the lowest layer infinitely deep and at rest. The purpose is to illustrate the profound impact of the bottom topography and the barotropic mode using results from otherwise identical

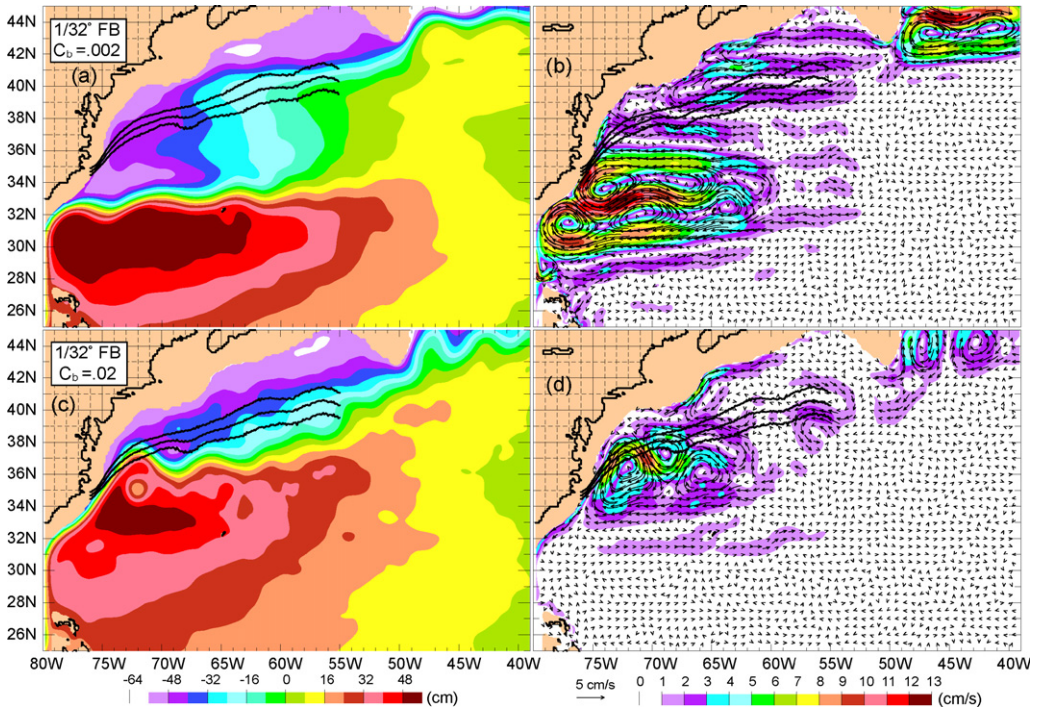


Fig. 9. Results from $1/32^\circ$ flat bottom simulations (depth = 6500 m) that are otherwise identical in design to the $1/32^\circ$ simulations with a DWBC shown in Figs. 2 and 3. (a) and (b) With $C_b = .002$ are flat bottom analogs of Figs. 2c and 3c. (c) and (d) With $C_b = .02$ are flat bottom analogs of Figs. 2e and 3e.

models. Flat bottom analogs of all the simulations shown in Fig. 2 were performed, but the results for the analogs of Fig. 2a–d were so similar that only the analog of Fig. 2c ($1/32^\circ$ with a DWBC) is shown in Fig. 9a and b. Likewise, the DWBC had little impact on the flat bottom simulations with $C_b = .02$ and only the simulation with a DWBC is used in Fig. 9c and d.

All four of the flat bottom simulations with $C_b = .002$ separate from the coast at the same latitude (32.5°N) and generate a nearly zonal jet along the same latitude ($\sim 33^\circ\text{N}$), several degrees south of the observed pathway (Fig. 9a) and 2.5° south of 35.5°N , the center of the broad wind-driven eastward current in the linear solution (Fig. 1). Doubling the resolution and removing the DWBC each add $\sim 4\text{--}5^\circ$ to the eastward penetration of the zonal jet. The same occurs for the eddy-driven counter-rotating, zonally oriented abyssal recirculation gyres. The current along the common boundary of these gyres flows eastward directly beneath the surface jet (Fig. 9b), exhibiting the same barotropic mean vertical structure for baroclinically unstable zonal jets found in the flat bottom double gyre model of Holland and Lin (1975), but unlike the present example, their zonal jet follows the zero wind stress curl line. In the surface layer there is a robust recirculation gyre on the south side of the eastward surface jet, but only a weak one on the north side. In the simulation depicted in Fig. 9a, some residual mean flow continues northward along the western boundary north of the zonal jet, as in the linear solution (Fig. 1). The other three simulations with $C_b = .002$ show the same feature except that the flow separates from the boundary over a 2° segment north of the zonal jet. The remainder of the mean northward flow (MOC + wind-driven) occurs as a broad, generally meridional interior flow, unlike the linear solution (Fig. 1), where it occurs along the western boundary. The upper ocean mesoscale variability north of the zonal jet between 33°N and 40°N is so chaotic in instantaneous snapshots (not shown) that there is little zonal rectification in the mean and little mean interior flow that reaches the western boundary, thus resulting in the broad mean northward upper ocean interior flow.

The flat bottom simulation is improved when $C_b = .02$ is used (Fig. 9c) and the abyssal circulation is greatly weakened. The resulting mean surface jet and associated abyssal circulation are less zonal and farther north. However, as with the corresponding flat bottom simulation with $C_b = .002$ (Fig. 9a), the boundary current separation is not complete and part of it continues along the boundary north of the main separation point. There is only a tiny northern recirculation gyre and it does not extend to the western boundary.

The two-layer theory for abyssal current steering of upper ocean current pathways, presented in Section 2, can also be used to explain certain features of the mean circulation in the flat bottom experiments, but this time without topographic constraints on the pathways of abyssal currents and without the resulting topographic impacts on the simulated pathway of the Gulf Stream. First, it can be used to explain the barotropic nature of the relatively strong mean circulation features, particularly evident for the eastward jets representing the model simulations of the Gulf Stream. In the two-layer theory, abyssal current advection of upper ocean current pathways ceases when these currents are parallel, resulting in a natural tendency toward barotropy, barring some aspect of the flow that prevents it.

The premature western boundary current separation seen in Exp. $1/32^\circ$ -9a (Fig. 9a) is not due to numerical inaccuracy (Verron and Blayo, 1996) or the DWBC, as demonstrated by the insensitivity to $1/16^\circ$ versus $1/32^\circ$ resolution and corresponding simulations with and without a DWBC. The viscous sublayer is well resolved as noted in Section 2. The bottom friction is the only difference between the flat bottom simulations illustrated in Fig. 9, yet the simulation in Fig. 9a and b (Exp. $1/32^\circ$ -9a) exhibits premature separation from the western boundary while the primary separation in Fig. 9c and d (Exp. $1/32^\circ$ -9c) occurs at the observed latitude with inertial jet characteristics influenced by the angle of the coastline. The difference in the separation latitude results from the impact of the bottom friction coefficient (C_b) on the eddy-driven mean abyssal circulation. In Fig. 9b the mean abyssal gyres are stronger and there is a well-developed cyclonic northern gyre that extends to the western boundary. Since the western boundary is farther to the west at lower latitudes in this area, the southward boundary current of the northern gyre lies east of the northward boundary current of the anticyclonic southern gyre. As a result the southward boundary current of the northern abyssal gyre intersects with the simulated Gulf Stream just east of the western boundary and thus can advect it southward.

In the simulation with $C_b = .02$ (Fig. 9d) the eddy-driven mean abyssal gyres are weaker. In addition, the cyclonic northern abyssal gyre does not extend to the western boundary and thus lacks the abyssal current steering that caused premature separation in the simulation with $C_b = .002$. However, the dynamics of the separating jets are very different in the simulations with realistic bottom topography (Figs. 2 and 3) and the flat bottom simulation with $C_b = .02$ in Fig. 9c and d. The former exhibit a relatively stable jet with CAV-like dynamics between separation from the western boundary and $\sim 70^\circ$ W (Fig. 6), while the latter demonstrates strong baroclinic instability, as evidenced by high surface and abyssal EKE (not shown) and the eddy-driven mean abyssal gyre directly beneath the first mean meander of the separating jet.

In the flat bottom simulations, the pathway of the simulated Gulf Stream and the associated eddy-driven abyssal currents tend to have a barotropic phase relationship that is continuous over a substantial distance (Fig. 9). That is prevented in the simulations with realistic bottom topography. However, the mean upper ocean and abyssal currents in the simulations with the topography do exhibit multiple segments with a nearly barotropic relationship, i.e. the currents are coherent in the vertical, but often tilt with depth. Thus, a given vertical cross-section of the Gulf Stream may exhibit a vertically coherent current from the surface to the seafloor, but that vertical structure is continuous over a much shorter distance than in the flat bottom simulations (Figs. 2, 3, and 4a versus Fig. 9).

Would completely eliminating the abyssal circulation and baroclinic instability involving the barotropic mode improve the results over those seen in the flat bottom simulations? That is addressed using a corresponding $1/32^\circ$ reduced-gravity simulation where the lowest layer is infinitely deep and at rest. In this case the mean flow (Fig. 10a) depicts the basic features of the linear solution shown in Fig. 1 with (1) an eastward interior current generally following the central latitude (35.5° N) demanded by Sverdrup flow and (2) the northward continuation of a current along the western boundary. In addition, there are two unrealistic mean recirculation gyres along the western boundary region, the one near 35° N associated with overshoot north of 35.5° N as the eastward branch separates from the coast,

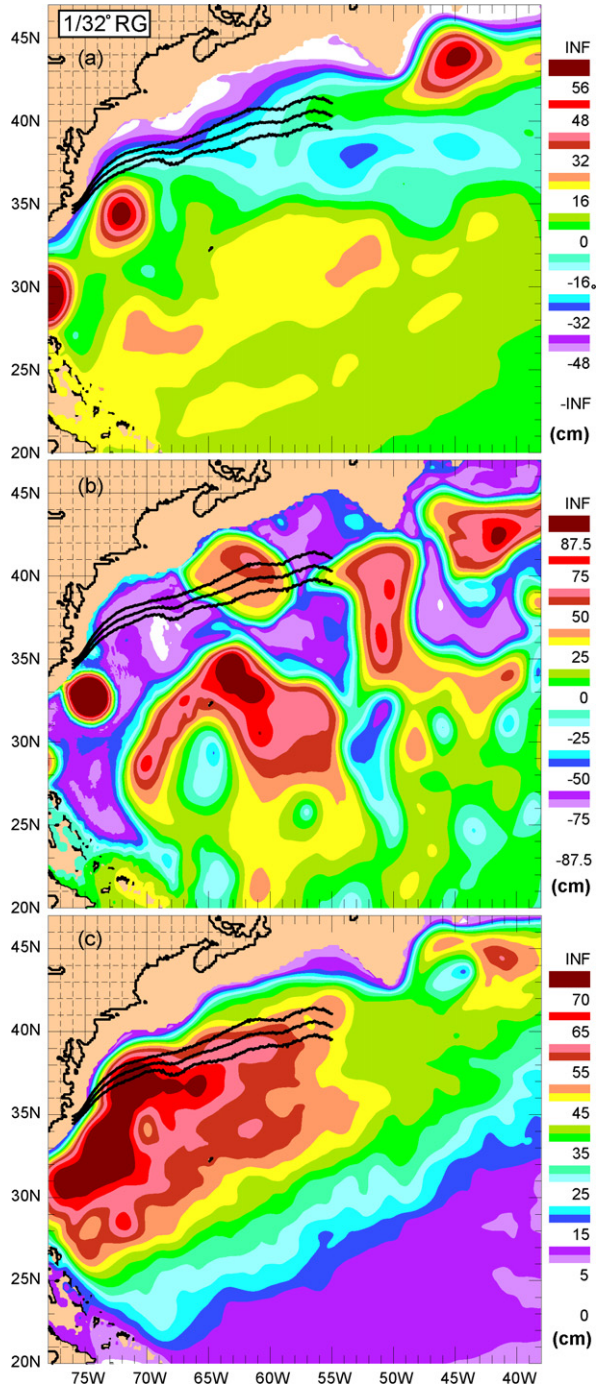


Fig. 10. Results from a $1/32^\circ$, 4.5 layer reduced-gravity simulation that is otherwise identical in design to the $1/32^\circ$ simulation without a DWBC shown in Fig. 2d, but with the 5th layer infinitely deep and at rest (thus no bottom friction) in the 4.5 layer simulation. (a) 10-Year mean SSH, (b) snapshot of SSH and (c) RMS SSH variability over a 10-year period (contour interval = 8, 12.5, and 5 cm in panels a, b, and c, respectively).

but an overshoot that is actually more consistent with the observed separation (IR northwall overlaid) than the linear solution. In contrast, an instantaneous snapshot looks very different from the mean and depicts a single narrow jet meandering wildly across the basin (Fig. 10b). Larger time and space scales are associated with reduced-gravity simulations with multiple active layers than are found in finite depth simulations. Correspondingly, the SSH variability is much larger than observed (Fig. 7) or than seen in the finite depth simulations (see Hurlburt and Hogan, 2000, their Fig. 9) and it covers a much larger region, showing the areal extent of the wildly meandering current and associated large eddies (Fig. 10c). Multilayer reduced-gravity simulations allow barotropic and internal mode baroclinic instabilities but exclude baroclinic instabilities involving the barotropic mode that would give smaller space and time scales, e.g. see a comparison of simulations with different design characteristics and dynamics for the Kuroshio in Hurlburt et al. (1996).

5. Summary and conclusions

A hydrodynamic model with five Lagrangian layers in the vertical was used to investigate the dynamics of Gulf Stream separation from the western boundary at Cape Hatteras and its mean pathway to the Grand Banks. The model domain covers the subtropical Atlantic basin and the Intra-Americas Sea from 9°N to 47°N. The model design is intermediate between highly idealized and a complex OGCM designed for comprehensive simulation of ocean processes, thus facilitating computational feasibility, experimental design and interpretation of the dynamics. However, it is realistic enough to permit detailed model-data comparisons that are used in assessing the model dynamics and their relevance in explaining Gulf Stream separation from the western boundary and its pathway to the east. In particular, the model is designed to allow realistic boundary geometry, bathymetry, wind forcing, and a meridional overturning circulation (MOC), the latter specified via ports in the northern and southern boundaries. More precisely, the model used vertically compressed but otherwise realistic topography confined to the bottom layer. Given 1/16° (~7 km) mid-latitude resolution or finer, Hurlburt and Hogan (2000) demonstrated that the model (configured with all of the preceding features and a 14 Sv MOC) performed well in a wide range of model-data comparisons, including the mean pathway of the Gulf Stream.

In the Gulf Stream region we investigated the impacts of the Deep Western Boundary Current (DWBC) and the eddy-driven mean abyssal circulation on Gulf Stream separation from the coast and its pathway to the Grand Banks. These impacts were investigated using 1/16° and 1/32° models with and without a DWBC, but with the northward upper ocean flow of the MOC included in all of the simulations. The 1/32° model was also run with standard and 10× higher bottom friction, with and without a DWBC in both cases. In addition, each simulation was run with realistic bottom topography and a flat bottom, and it was run in reduced-gravity mode when applicable. The corresponding linear solution with a Sverdrup interior and Munk viscous western boundary layers (including a western boundary layer driven by the northward upper ocean flow of the MOC) yields two unrealistic Gulf Stream pathways, a broad wind-driven pathway flowing due east from Cape Hatteras (centered along 35.5°N) and an MOC pathway plus a second wind-driven pathway that both hug the western boundary all the way to the Grand Banks, except for a zonal connecting segment along 42–43°N. An ocean model with high horizontal resolution is required to avoid this problem by simulating a single nonlinear Gulf Stream pathway that separates from the coast.

In the model simulations (1) a sufficiently inertial Gulf Stream and (2) a strong eddy-driven mean abyssal circulation constrained by realistic topography were necessary and sufficient to obtain a realistic Gulf Stream pathway. The 1/32° simulations with realistic bottom topography and normal bottom friction yielded nearly identical realistic mean Gulf Stream pathways with and without a DWBC except southeast of the Grand Banks. One key dynamical process is upper ocean – topographic coupling via flow instabilities, where topographically constrained eddy-driven mean abyssal currents help steer the mean pathways of upper ocean currents that do not directly impinge on the topography. In two cases with realistic bottom topography, the 1/16° model and the 1/32° model with high bottom friction, the simulated eddy-driven abyssal circulation alone was not strong enough to prevent simulation overshoot of the observed latitude of the Gulf Stream pathway between the coast and 68°W. In these two cases the DWBC contribution to the steering of upper ocean current pathways was crucial in sim-

ulating realistic Gulf Stream separation from the coast, demonstrating that the conclusions one might draw about the role of the DWBC in Gulf Stream separation could be model resolution dependent. In the corresponding $1/8^\circ$ simulation with a DWBC, the eddy-driven mean abyssal circulation was almost nonexistent and the simulated Gulf Stream pathway was unrealistic even with a DWBC. The DWBC does play an essential role in simulation of the outer of two mean surface current meanders around the Southeast Newfoundland Rise, where the Gulf Stream transitions to the North Atlantic Current as it rounds the Grand Banks, a phenomenon seen even in the $1/8^\circ$ model.

Otherwise identical simulations performed with a flat bottom or a reduced-gravity model are much different than the simulations with topography. Abyssal current steering of upper ocean current pathways was used to explain (1) why the flat bottom simulation with standard bottom friction exhibited severe premature separation from the western boundary while the simulation with high bottom friction did not and (2) the relative barotropy of the mean flow in the flat bottom simulations compared to those with topography. The reduced-gravity simulations yielded mean Gulf Stream pathways consistent with the linear solution, but with the addition of a small nonlinear recirculation gyre where the stream separated from the coast that did not cause overshoot of the observed separation latitude. Unlike the finite depth simulations, the reduced-gravity model gave instantaneous snapshots of the Gulf Stream pathway that were extremely different from the mean. The simulated stream exhibited a narrow jet with wild meanders that spanned most of the subtropical gyre.

Both the capability to evaluate the accuracy of the simulations through model-data comparisons and the assessed realism of the $1/16^\circ$ and $1/32^\circ$ simulations with realistic topography were sufficient to allow a detailed investigation of Gulf Stream dynamics, including its separation from the western boundary and its pathway to the east. East of 68°W all six of the simulations in Fig. 2 exhibited similar generally realistic pathways that were influenced by eddy-driven abyssal current steering. West of 68°W four of the six simulations exhibited realistic Gulf Stream pathways and in two of the three with no DWBC the simulated Gulf Stream pathway overshoot the observed separation latitude. At a given resolution these differences are not due to differences in the inertial character of the simulations. The mean speed at the core of the stream is consistent with observations near its separation from the western boundary in all six of the simulations depicted in Fig. 2. Despite this agreement, none of the simulated Gulf Streams were sufficiently inertial to overcome the constraint of the linear solution for flow north of the observed separation latitude without assistance from abyssal current steering of the pathway.

The key abyssal current crosses under the Gulf Stream at $68.5\text{--}69^\circ\text{W}$. Given sufficient strength (threshold of $\sim 4\text{ cm s}^{-1}$) this current advects the pathway of the Gulf Stream southward to the terminus of an escarpment in the continental slope. There the isobaths diverge and part of the current continues westward along the continental slope and the northern edge of the Gulf Stream, while the remainder crosses under the stream. The latter crosses to deeper depths in order to conserve potential vorticity while passing under the downward slope across the base of the Gulf Stream thermocline, a phenomenon theorized by Hogg and Stommel (1985) and first verified observationally by Pickart and Watts (1990). Positive relative vorticity is generated while the abyssal current passes under the stream, and after passing under the stream, the abyssal current immediately retroreflects eastward onto the abyssal plain, thus eliminating the component of flow normal to the stream and preventing further southward abyssal current advection of the Gulf Stream pathway. As a result, specific features of the bottom topography and feedback from the influence of the Gulf Stream on the abyssal current pathway determined the latitude of the stream at $68.5\text{--}69^\circ\text{W}$. The speed and direction of the associated abyssal currents are consistent with those observed by Johns et al. (1995).

West of 69°W the observed and modeled Gulf Stream pathways are relatively stable and with the assistance of the abyssal current at $68.5\text{--}69^\circ\text{W}$ the stream pathway between the western boundary and $\sim 70^\circ\text{W}$ is in close agreement with a constant absolute vorticity (CAV) trajectory that is strongly influenced by the angle of the coastline prior to Gulf Stream separation. Additional abyssal currents pass under the stream farther to the west, but have little effect on its pathway, one near 75°W because it is nearly anti-parallel where it crosses under the stream, consistent with observations (Pickart, 1994). Another crosses under the Gulf Stream at $71\text{--}73^\circ\text{W}$. It depends on the DWBC for its existence, but is locally augmented by a stronger eddy-driven contribution. It is strong enough to have a noticeable

effect on the stream pathway only in the $1/32^\circ$ simulation with a DWBC and standard bottom friction. It passes under the stream in a manner similar to the current at $68.5\text{--}69^\circ\text{W}$, but the latitude of the stream resulting from this mechanism is only a small perturbation from that predicted by the CAV trajectory. Thus the CAV trajectories and the constraint on the latitude of the Gulf Stream pathway at $68.5\text{--}69^\circ\text{W}$ work together in determining the simulated Gulf Stream pathways between the western boundary and 68°W . Neither alone is sufficient to explain the Gulf Stream pathway in that region.

It is worthy of note that the explanation for the mean Gulf Stream pathway is the same for the four simulations with a realistic pathway except for the effect of the DWBC on the strength of the crucial abyssal current crossing under the Gulf Stream at $68.5\text{--}69^\circ\text{W}$. This crucial abyssal current appears only in simulations with an eddy-driven abyssal circulation. In the $1/16^\circ$ simulation and the $1/32^\circ$ simulation with a high bottom friction, the DWBC increases the strength of the crucial abyssal current above the threshold ($\sim 4\text{ cm s}^{-1}$) required for sufficient abyssal current steering of the Gulf Stream pathway at that location. In the $1/32^\circ$ simulation with standard bottom friction, the strength of this abyssal current is slightly reduced by adding a DWBC, but its strength remains well above the threshold. Increasing the strength above the threshold has little effect because, above the threshold the latitude of the Gulf Stream at that location is not determined by the strength of the advection, as discussed earlier. This result and its assistance in achieving a CAV trajectory for the Gulf Stream pathway west of $\sim 70^\circ\text{W}$ explain the robust agreement of the mean simulated pathways in the four simulations with a realistic pathway west of 68°W as well as their close agreement with the observed mean IR northwall pathway, despite their differences in resolution, bottom friction, strength of the abyssal circulation, and presence or absence of a DWBC.

Acknowledgements

This article is a contribution to the projects “Global Remote Littoral Forcing via Deep Water Pathways” and “Data Assimilation and Model Evaluation Experiment – North Atlantic Basin (DAMEE–NAB)” sponsored by the Office of Naval Research (ONR) under program elements 601153N and 602435N, respectively. Grants of both “challenge” and “non-challenge” computer time were provided by the Dept. of Defense High Performance Computing Modernization Program. We thank guest editor, Igor Belkin, for his invitation to write an article for this special issue. We also thank Alan Wallcraft for his computer expertise and his developmental work on the NRL Layered Ocean Model (NLOM). We thank Gregg Jacobs (NRL) for providing the along-track satellite altimeter SSH variability analysis. We thank the reviewers for useful comments that lead to significant improvements in the manuscript. We also thank Charlene Parker, Jay Shriver and Luis Zamudio for their assistance. The mean Gulf Stream northwall pathway, based on satellite infrared imagery, is an unpublished analysis performed by Peter Cornillon (University of Rhode Island) and Ziv Sirkes (deceased) for the ONR project DAMEE–NAB. This is Naval Research Laboratory publication number NRL/JA/7304-08-8080.

References

- Auer, S.J., 1987. Five-year climatological survey of the Gulf Stream system and its associated rings. *J. Geophys. Res.* 92 (C11), 11709–11726.
- Bower, A.S., Hunt, H.D., 2000a. Lagrangian observations of the Deep Western Boundary Current in the North Atlantic Ocean. Part I. Large-scale pathways and spreading rates. *J. Phys. Oceanogr.* 30, 764–783.
- Bower, A.S., Hunt, H.D., 2000b. Lagrangian observations of the Deep Western Boundary Current in the North Atlantic Ocean. Part II. The Gulf Stream–Deep Western Boundary Current crossover. *J. Phys. Oceanogr.* 30, 784–804.
- Bryan, F.O., Hecht, M.W., Smith, R.D., 2007. Resolution convergence and sensitivity studies with North Atlantic circulation models. Part I. The western boundary current system. *Ocean Model.* 16, 141–159.
- Cayula, J.F., Cornillon, P., 1995. Multi-image edge detection for SST images. *J. Atmos. Oceanic Technol.* 12, 821–829.
- Chassignet, E.P., Marshall, D.P., 2008. Gulf Stream separation in numerical ocean models. In: Hecht, M.W., Hasumi, H. (Eds.), *Ocean Modeling in an Eddy Regime*. Geophysical Monograph 177, American Geophysical Union, Washington, DC.
- Cornillon, P., 1986. The effect of the New England Seamounts on Gulf Stream meandering as observed from satellite IR images. *J. Phys. Oceanogr.* 16, 386–389.
- Dengg, J., 1993. The problem of Gulf Stream separation: a barotropic approach. *J. Phys. Oceanogr.* 23, 2182–2200.
- Dengg, J., Beckmann, A., Gerdes, R., 1996. The Gulf Stream separation problem. In: Krauss, W. (Ed.), *The Warmwatersphere of the North Atlantic Ocean*. Gebr. Borntraeger, Berlin, pp. 253–290.
- Godfrey, J.S., 1989. A Sverdrup model of the depth-integrated flow for the world ocean allowing for island circulations. *Geophys. Astrophys. Fluid Dyn.* 45 (1–2), 89–112.

- Halkin, D., Rossby, H.T., 1985. The structure and transport of the Gulf Stream at 73°W. *J. Phys. Oceanogr.* 15 (11), 1439–1452.
- Haltiner, G.J., Martin, F.L., 1957. *Dynamical and Physical Meteorology*. McGraw-Hill, New York.
- Hellerman, S., Rosenstein, M., 1983. Normal monthly wind stress over the world ocean with error estimates. *J. Phys. Oceanogr.* 13, 1093–1104.
- Hogan, P.J., Hurlburt, H.E., 2000. Impact of upper ocean – topographic coupling and isopycnal outcropping in Japan/East Sea models with 1/8° to 1/64° resolution. *J. Phys. Oceanogr.* 30, 2535–2561.
- Hogan, P.J., Hurlburt, H.E., 2005. Sensitivity of simulated circulation to surface wind forcing in the Japan/East Sea. *Deep Sea Res.* 52, 1464–1489.
- Hogg, N.G., Stommel, H., 1985. On the relation between the deep circulation and the Gulf Stream. *Deep Sea Res.* 32, 1181–1193.
- Holland, W.R., Lin, L.B., 1975. On the generation of mesoscale eddies and their contribution to the oceanic general circulation. 2. A parameter study. *J. Phys. Oceanogr.* 5 (4), 658–669.
- Hurlburt, H.E., Hogan, P.J., 2000. Impact of 1/8° to 1/64° resolution on Gulf Stream model-data comparisons in basin-scale subtropical Atlantic Ocean models. *Dyn. Atmos. Oceans* 32, 283–329.
- Hurlburt, H.E., Metzger, E.J., 1998. Bifurcation of the Kuroshio Extension at the Shatsky Rise. *J. Geophys. Res.* 103, 7549–7566.
- Hurlburt, H.E., Metzger, E.J., Hogan, P.J., Tilburg, C.E., Shriver, J.F., 2008. Steering of upper ocean currents and fronts by the topographically-constrained abyssal circulation. *Dyn. Atmos. Oceans* 45, 102–134.
- Hurlburt, H.E., Thompson, J.D., 1980. A numerical study of Loop Current intrusions and eddy shedding. *J. Phys. Oceanogr.* 10, 1611–1651.
- Hurlburt, H.E., Thompson, J.D., 1982. The dynamics of the Loop Current and shed eddies in a numerical model of the Gulf of Mexico. In: Nihoul, J.C.J. (Ed.), *Hydrodynamics of Semi-Enclosed Seas*. Elsevier, Amsterdam, pp. 243–297.
- Hurlburt, H.E., Thompson, J.D., 1984. Preliminary results from a numerical study of the New England Seamount Chain influence on the Gulf Stream. In: Holloway, G., West, B.J. (Eds.), *Predictability of Fluid Motions*, Amer. Inst. Physics Conf. Proc. 106. American Institute of Physics, New York, pp. 489–503.
- Hurlburt, H.E., Wallcraft, A.J., Schmitz Jr., W.J., Hogan, P.J., Metzger, E.J., 1996. Dynamics of the Kuroshio/Oyashio current system using eddy-resolving models of the North Pacific Ocean. *J. Geophys. Res.* 101 (C1), 941–976.
- Johns, W.E., Shay, T.J., Bane, J.M., Watts, D.R., 1995. Gulf Stream structure, transport, and recirculation near 68°W. *J. Geophys. Res.* 100 (C1), 817–838.
- Joyce, T.M., Wunsch, C., Pierce, S.D., 1986. Synoptic Gulf Stream velocity profiles through simultaneous inversion of hydrographic and acoustic Doppler data. *J. Geophys. Res.* 91 (C6), 7573–7585.
- Kearns, E.J., Rossby, H.T., 1998. Historical position of the North Atlantic Current. *J. Geophys. Res.* 103 (C8), 15509–15524.
- Kraus, E.B., Turner, J.S., 1967. A one-dimensional model of the seasonal thermocline. II. The general theory and its consequences. *Tellus* 19, 98–106.
- Lee, H., 1997. A Gulf Stream synthetic geoid for the TOPEX altimeter. M.S. Thesis. Rutgers University, New Brunswick, NJ.
- Lee, T., Cornillon, P., 1996. Propagation of Gulf Stream meanders between 74° and 70°W. *J. Phys. Oceanogr.* 26, 205–224.
- Levitus, S., 1982. *Climatological atlas of the world ocean*. NOAA Prof. Pap. 13. U.S. Govt. Print. Off., Washington, DC.
- McManus, A.P., Townsend, T.L., Metzger, E.J., 1997. Creation and modification of 1/8° and 1/16° subtropical gyre Atlantic topographies. NRL FR, 7323-95-9626. Nav. Res. Lab., Stennis Space Center, MS.
- Metzger, E.J., Hurlburt, H.E., 1996. Coupled dynamics of the South China Sea, the Sulu Sea, and the Pacific Ocean. *J. Geophys. Res.* 101 (C5), 12331–12352.
- Moore, D.R., Wallcraft, A.J., 1998. Formulation of the NRL Layered Ocean Model in spherical coordinates. NRL CR 7323-96-0005. Nav. Res. Lab., Stennis Space Center, MS.
- Munk, W.H., 1950. On the wind-driven ocean circulation. *J. Met.* 7 (2), 79–93.
- National Oceanic and Atmospheric Administration (NOAA), 1986. ETOPO5 digital relief of the surface of the earth. Data Announcement 86-MGG-07. Natl. Geophys. Data Cent., Washington, DC.
- Özğökmen, T.M., Chassignet, E.P., Paiva, A.M., 1997. Impact of wind forcing, bottom topography, and inertia on midlatitude jet separation in a quasi-geostrophic model. *J. Phys. Oceanogr.* 27, 2460–2476.
- Paiva, A.M., Hargrove, J.T., Chassignet, E.P., Bleck, R., 1999. Turbulent behavior of a fine mesh (1/12°) numerical simulation of the North Atlantic. *J. Mar. Syst.* 21, 307–320.
- Pickart, R.S., 1994. Interaction of the Gulf Stream and Deep Western Boundary Current where they cross. *J. Geophys. Res.* 99 (C12), 25155–25164.
- Pickart, R.S., Watts, D.R., 1990. Deep Western Boundary Current variability at Cape Hatteras. *J. Mar. Res.* 48, 765–791.
- Reid, R.O., 1972. A simple dynamic model of the Loop Current. In: Capurro, L.R.A., Reid, J.L. (Eds.), *Contributions on the Physical Oceanography of the Gulf of Mexico*, Vol. II. Gulf Publishing Co., Houston, TX, pp. 157–159.
- Rossby, C.-G., 1940. Planetary flow patterns in the atmosphere. *Quart. J. Roy. Meteorol. Soc.*, Suppl. 66, 68–87.
- Schmitz, W.J., 1996. On the world ocean circulation. Volume I. Some Global Features/North Atlantic Circulation, Technical Report WHOI-96-03. Woods Hole Oceanographic Institution, Woods Hole, MA.
- Schmitz Jr., W.J., McCartney, M.S., 1993. On the North Atlantic circulation. *Rev. Geophys.* 31 (1), 29–49.
- Schmitz Jr., W.J., Thompson, J.D., 1993. On the effects of horizontal resolution in a limited-area model of the Gulf Stream system. *J. Phys. Oceanogr.* 23, 1001–1007.
- Shriver, J.F., Hurlburt, H.E., Smedstad, O.M., Wallcraft, A.J., Rhodes, R.C., 2007. 1/32° real-time global ocean prediction and value-added over 1/16° resolution. *J. Mar. Syst.* 65 (1–4), 3–26.
- Smedstad, O.M., Hurlburt, H.E., Metzger, E.J., Rhodes, R.C., Shriver, J.F., Wallcraft, A.J., Kara, A.B., 2003. An operational eddy-resolving 1/16° global ocean nowcast/forecast system. *J. Mar. Syst.* 40–41, 341–361.
- Smith, R.D., Maltrud, M.E., Bryan, F.O., Hecht, M.W., 2000. Numerical simulation of the North Atlantic Ocean at 1/10°. *J. Phys. Oceanogr.* 30, 1532–1561.
- Spall, M.A., 1996a. Dynamics of the Gulf Stream/Deep Western Boundary Current crossover. Part I. Entrainment and recirculation. *J. Phys. Oceanogr.* 26, 2152–2168.
- Spall, M.A., 1996b. Dynamics of the Gulf Stream/Deep Western Boundary Current crossover. Part II. Low-frequency internal oscillations. *J. Phys. Oceanogr.* 26, 2169–2182.

- Sverdrup, H.U., 1947. Wind-driven currents in a baroclinic ocean—with application to the equatorial currents of the eastern Pacific. *Proc. Natl. Acad. Sci. U.S.A.* 33 (11), 318–326.
- Teague, W.J., Carron, M.J., Hogan, P.J., 1990. A comparison between the generalized digital environmental model and the Levitus climatology. *J. Geophys. Res.* 95 (C5), 7167–7183.
- Thompson, J.D., Schmitz Jr., W.J., 1989. A regional primitive-equation model of the Gulf Stream: design and initial experiments. *J. Phys. Oceanogr.* 19, 791–814.
- Tilburg, C.E., Hurlburt, H.E., O'Brien, J.J., Shriver, J.F., 2001. The dynamics of the East Australian Current system: the Tasman Front, the East Auckland Current and the East Cape Current. *J. Phys. Oceanogr.* 31, 2917–2943.
- Townsend, T.L., Hurlburt, H.E., Hogan, P.J., 2000. Modeled Sverdrup flow in the North Atlantic from 11 different wind stress climatologies. *Dyn. Atmos. Oceans* 32, 373–417.
- Verron, J., Blayo, E., 1996. The no-slip condition and separation of western boundary currents. *J. Phys. Oceanogr.* 26, 1938–1951.
- Wallcraft, A.J., 1991. The Navy Layered Ocean Model Users Guide. NOARL Report 35. Nav. Res. Lab., Stennis Space Center, MS.
- Wallcraft, A.J., Kara, A.B., Hurlburt, H.E., 2005. Convergence of Laplacian diffusion versus resolution of an ocean model. 32:L07604, doi:10.1029/2005GL022514.
- Wallcraft, A.J., Kara, A.B., Hurlburt, H.E., Rochford, P.A., 2003. The NRL Layered Ocean Model (NLOM) with an embedded mixed layer sub-model: formulation and tuning. *J. Atmos. Oceanic Technol.* 20, 1601–1615.
- Wallcraft, A.J., Moore, D.R., 1997. The NRL Layered Ocean Model. *Parall. Comput.* 23, 2227–2242.
- Watts, D.R., Tracey, K.L., Bane, J.M., Shay, T.J., 1995. Gulf Stream path and thermocline structure near 74°W and 68°W. *J. Geophys. Res.* 100 (C9), 18291–18312.